Probabilistic Engineering Mechanics 60 (2020) 103044

Contents lists available at ScienceDirect

Probabilistic Engineering Mechanics

journal homepage: www.elsevier.com/locate/probengmech

Stochastic response determination of nonlinear structural systems with singular diffusion matrices: A Wiener path integral variational formulation with constraints

Ioannis Petromichelakis, Apostolos F. Psaros, Ioannis A. Kougioumtzoglou *

Department of Civil Engineering and Engineering Mechanics, Columbia University, 500 W 120th St, New York, NY 10027, United States

ARTICLE INFO

Keywords:
Singular diffusion matrix
Path integral
Constrained variational problem
Stochastic dynamics
Nonlinear system

ABSTRACT

The Wiener path integral (WPI) approximate semi-analytical technique for determining the joint response probability density function (PDF) of stochastically excited nonlinear oscillators is generalized herein to account for systems with singular diffusion matrices. Indicative examples include (but are not limited to) systems with only some of their degrees-of-freedom excited, hysteresis modeling via additional auxiliary state equations, and energy harvesters with coupled electro-mechanical equations. In general, the governing equations of motion of the above systems can be cast as a set of underdetermined stochastic differential equations coupled with a set of deterministic ordinary differential equations. The latter, which can be of arbitrary form, are construed herein as constraints on the motion of the system driven by the stochastic excitation. Next, employing a semi-classical approximation treatment for the WPI yields a deterministic constrained variational problem to be solved numerically for determining the most probable path; and thus, for evaluating the system joint response PDF in a computationally efficient manner. This is done in conjunction with a Rayleigh-Ritz approach coupled with appropriate optimization algorithms. Several numerical examples pertaining to both linear and nonlinear constraint equations are considered, including various multi-degree-of-freedom systems, a linear oscillator under earthquake excitation and a nonlinear oscillator exhibiting hysteresis following the Bouc–Wen formalism. Comparisons with relevant Monte Carlo simulation data demonstrate a relatively high degree of accuracy.

1. Introduction

Accurate response analysis of engineering dynamical systems necessitates an increasingly sophisticated modeling of the system behavior and of the associated excitations. This includes consideration of strong nonlinearities, complex hysteresis, stochastic loads, as well as a relatively high dimensionality of the system response vector. Despite their versatility and implementation simplicity, the performance of purely numerical solution techniques, such as various Monte Carlo simulation (MCS) schemes (e.g., [1,2]), for determining the system stochastic response is often hindered by the related excessive computational cost. In this regard, alternative semi-analytical methodologies, such as the recently developed Wiener path integral (WPI) technique [3,4], exhibit both a satisfactory accuracy degree and a tractable computational cost. In particular, the WPI solution technique, which relies on functional integration concepts and on a variational formulation, is capable of determining the joint response transition probability density function (PDF) of stochastically excited multi-degree-of-freedom (MDOF) nonlinear systems, even when endowed with fractional derivative terms (e.g., [3–5]). Further, it can account for diverse non-white and non-Gaussian stochastic process modeling [6], while it has been shown recently that the associated computational cost can be drastically reduced by employing sparse representations for the system response PDF in conjunction with compressive sampling schemes and group sparsity concepts (e.g., [7–9]).

Nevertheless, the applicability of the WPI technique has so far been restricted to systems with non-singular diffusion matrices. In fact, the general formulation of the technique involving the inversion of the governing equation diffusion matrix does not allow for a straightforward extension to cases pertaining to singular diffusion matrices, and thus, special mathematical treatments are required (e.g., [10–12]). Indicative examples, where such special treatments can be rather trivial, include casting the higher-order (e.g., second-order) governing equation into a lower-order (e.g., first-order) form by introducing additional state variables, as well as modeling non-white excitations via filter equations (e.g., [6,13,14]). In such cases, the limitation of singular diffusion matrices can be readily bypassed (e.g., [15]) by enforcing compatibility conditions of a rather simple (almost trivial) form between the

* Corresponding author.
E-mail address: ikougioum@columbia.edu (I.A. Kougioumtzoglou).

https://doi.org/10.1016/j.probengmech.2020.103044
Received 15 January 2020; Accepted 31 January 2020
Available online 7 February 2020

auxiliary variables and the time-derivatives of the original variables. However, this is not always the case as these auxiliary equations are more than often of a complex form. Examples include (but are not limited to) dynamical systems with only some of their DOFs forced, hysteretic models (e.g., Bouc–Wen [16]) with nonlinear auxiliary differential equations, and diverse energy harvesting systems such as various electromechanical harvesters (e.g., [17]) and wave energy converters (e.g., [18]).

In this paper, the WPI solution technique is generalized to cope with a broad class of systems with singular diffusion matrices. In this regard, the governing equations of motion are represented herein as a set of underdetermined stochastic differential equations (SDEs) coupled with a set of deterministic ordinary differential equations (ODEs). The latter, which can be of arbitrary (nonlinear) form, are construed as constraints on the motion of the system driven by the stochastic excitation (e.g., [19–21]). This yields a constrained variational problem to be solved for the most probable path, and thus, the system joint response PDF is determined. Several numerical examples pertaining to both linear and nonlinear constraint equations are considered, including MDOF systems with only some of their DOFs stochastically excited, a linear oscillator under Kanai–Tajimi earthquake excitation, as well as a nonlinear oscillator exhibiting hysteresis following the Bouc–Wen formalism. Direct comparisons with MCS data demonstrate a relatively high degree of accuracy.

2. Wiener path integral formalism aspects

2.1. Preliminaries

This section serves as a brief overview of several aspects of the theory of SDEs and the associated Chapman–Kolmogorov (C-K) and Fokker–Planck (F-P) equations. In this regard, consider a multi-dimensional first-order SDE of the general form

$$\dot{\boldsymbol{\alpha}} = \mathbf{A}(\boldsymbol{\alpha}, t) + \mathbf{B}(\boldsymbol{\alpha}, t)\boldsymbol{\eta}(t) \tag{1}$$

where the dot above a variable denotes differentiation with respect to time t and $\boldsymbol{\eta}(t)$ is a zero-mean and delta-correlated process of intensity one; i.e., $\mathbb{E}[\boldsymbol{\eta}(t)] = \mathbf{0}$ and $\mathbb{E}[\boldsymbol{\eta}(t)\boldsymbol{\eta}^{\mathrm{T}}(t+\tau)] = \mathbf{I}\delta(\tau)$ where $\mathbf{I}$ is the identity matrix, and $\delta(t)$ is the Dirac delta function. Certain existence and uniqueness conditions related to Eq. (1) dictate that the solution $\boldsymbol{\alpha} = [\alpha_j]_{n\times 1}$ is a Markov stochastic vector process [22,23], for which the C-K equation (e.g., [24])

$$p(\boldsymbol{\alpha}_{i+1}, t_{i+1}|\boldsymbol{\alpha}_{i-1}, t_{i-1}) = \int_{-\infty}^{\infty} p(\boldsymbol{\alpha}_{i+1}, t_{i+1}|\boldsymbol{\alpha}_i, t_i)p(\boldsymbol{\alpha}_i, t_i|\boldsymbol{\alpha}_{i-1}, t_{i-1})\mathrm{d}\boldsymbol{\alpha}_i \tag{2}$$

is satisfied for any $t_{i-1} < t_i < t_{i+1}$. In Eq. (2), $\boldsymbol{\alpha}_i = \boldsymbol{\alpha}(t_i)$ and $p(\boldsymbol{\alpha}_{i+1}, t_{i+1}|\boldsymbol{\alpha}_{i-1}, t_{i-1})$ denotes the transition PDF of the process $\boldsymbol{\alpha}(t)$. Next, if $\mathbf{A}$ and $\mathbf{B}$ are continuous functions of t, then $\boldsymbol{\alpha}$ is a diffusion process [22] and the following conditions hold true for any $\varepsilon > 0$ (e.g., [23,25]), i.e.,

$$(i)\quad \lim_{\Delta t\to 0}\int_{|\boldsymbol{\alpha}_{i+1}-\boldsymbol{\alpha}_i|<\varepsilon} p(\boldsymbol{\alpha}_{i+1}, t_{i+1}|\boldsymbol{\alpha}_i, t_i)\mathrm{d}\boldsymbol{\alpha}_{i+1} = 0 \tag{3}$$

$$(ii)\quad \lim_{\Delta t\to 0}\int_{|\boldsymbol{\alpha}_{i+1}-\boldsymbol{\alpha}_i|<\varepsilon} (\boldsymbol{\alpha}_{i+1}-\boldsymbol{\alpha}_i)p(\boldsymbol{\alpha}_{i+1}, t_{i+1}|\boldsymbol{\alpha}_i, t_i)\mathrm{d}\boldsymbol{\alpha}_{i+1} = \mathbf{A}(\boldsymbol{\alpha}_i, t_i) \tag{4}$$

$$(iii)\quad \lim_{\Delta t\to 0}\int_{|\boldsymbol{\alpha}_{i+1}-\boldsymbol{\alpha}_i|<\varepsilon} (\boldsymbol{\alpha}_{i+1}-\boldsymbol{\alpha}_i)(\boldsymbol{\alpha}_{i+1}-\boldsymbol{\alpha}_i)^{\mathrm{T}}p(\boldsymbol{\alpha}_{i+1}, t_{i+1}|\boldsymbol{\alpha}_i, t_i)\mathrm{d}\boldsymbol{\alpha}_{i+1} = \mathbf{B}(\boldsymbol{\alpha}_i, t_i)\mathbf{B}^{\mathrm{T}}(\boldsymbol{\alpha}_i, t_i) \tag{5}$$

where $\Delta t = t_{i+1} - t_i$. Further, employing the C-K Eq. (2) leads to the F-P Eq. (6) for the transition PDF $p = p(\boldsymbol{\alpha}_{i+1}, t_{i+1}|\boldsymbol{\alpha}_i, t_i)$, i.e.,

$$\frac{\partial p}{\partial t} = -\sum_j \frac{\partial}{\partial \alpha_j}\left(A_j(\boldsymbol{\alpha}, t)p\right) + \frac{1}{2}\sum_{j,k}\frac{\partial^2}{\partial \alpha_j \alpha_k}\left(\tilde{B}_{jk}(\boldsymbol{\alpha}, t)p\right) \tag{6}$$

where $\mathbf{A}(\boldsymbol{\alpha}, t) = [A_j(\boldsymbol{\alpha}, t)]_{n\times 1}$ is the drift vector, and $\tilde{\mathbf{B}}(\boldsymbol{\alpha}, t) = [\tilde{B}_{jk}(\boldsymbol{\alpha}, t)]_{n\times n} := \mathbf{B}(\boldsymbol{\alpha}, t)\mathbf{B}^{\mathrm{T}}(\boldsymbol{\alpha}, t)$ denotes the diffusion matrix (e.g., [22,23,26]), which is symmetric and positive semidefinite.

2.2. Wiener path integral and Lagrangian function

In this section, basic WPI formalism aspects are presented for completeness. The interested reader is directed to [27–31] for more details. In the limit $\Delta t \to 0$, and assuming a non-singular diffusion matrix $\tilde{\mathbf{B}}$, the transition PDF associated with a diffusion process $\boldsymbol{\alpha}(t)$ has been shown to admit a Gaussian distribution (e.g., [26]) of the form

$$p(\boldsymbol{\alpha}_{i+1}, t_{i+1}|\boldsymbol{\alpha}_i, t_i) = \left[\sqrt{(2\pi\Delta t)^n \det\left[\tilde{\mathbf{B}}(\boldsymbol{\alpha}_i, t_i)\right]}\right]^{-1} \times \cdots$$
$$\exp\left(-\frac{1}{2}\frac{\left[\boldsymbol{\alpha}_{i+1}-\boldsymbol{\alpha}_i-\Delta t\mathbf{A}(\boldsymbol{\alpha}_i, t_i)\right]^{\mathrm{T}}\left[\tilde{\mathbf{B}}(\boldsymbol{\alpha}_i, t_i)\right]^{-1}\left[\boldsymbol{\alpha}_{i+1}-\boldsymbol{\alpha}_i-\Delta t\mathbf{A}(\boldsymbol{\alpha}_i, t_i)\right]}{\Delta t}\right) \tag{7}$$

In passing, it is noted that the choice of Eq. (7) is not restrictive, and alternative non-Gaussian distributions can also be employed (e.g., [32,33]). Next, the probability that $\boldsymbol{\alpha}(t)$ follows a specific path $\bar{\boldsymbol{\alpha}}(t)$ can be expressed as the limiting case of the probability of the compound event

$$P[\bar{\boldsymbol{\alpha}}(t)] = \lim_{\substack{\Delta t\to 0\\ N\to\infty}} P\left[\bigcap_{i=1}^{N}\left\{\boldsymbol{\alpha}_i \in \left[\bar{\boldsymbol{\alpha}}_i, \bar{\boldsymbol{\alpha}}_i + [\mathrm{d}\alpha_{ji}]_{n\times 1}\right]\right\}\right] \tag{8}$$

In Eq. (8), the time is discretized into N time points (slices) Δt apart, while $\mathrm{d}\alpha_{ji}$ denotes the infinitesimal element along dimension j at time t_i. Loosely speaking, Eq. (8) represents the probability of the process to propagate through the infinitesimally thin tube surrounding $\bar{\boldsymbol{\alpha}}(t)$. In the following, considering deterministic initial conditions, and employing Eq. (7) and the Markovian property of $\boldsymbol{\alpha}(t)$, Eq. (8) becomes

$$\begin{aligned} P[\bar{\boldsymbol{\alpha}}(t)] &= \lim_{\substack{\Delta t\to 0\\ N\to\infty}}\left\{\prod_{i=1}^{N} p(\bar{\boldsymbol{\alpha}}_{i+1}, t_{i+1}|\bar{\boldsymbol{\alpha}}_i, t_i)\prod_{j=1}^{n}\mathrm{d}\alpha_{ji}\right\} \\ &= \lim_{\substack{\Delta t\to 0\\ N\to\infty}}\left\{\left[\prod_{i=1}^{N}\left(\left[\sqrt{(2\pi\Delta t)^n\det\left[\tilde{\mathbf{B}}(\bar{\boldsymbol{\alpha}}_i, t_i)\right]}\right]^{-1}\prod_{j=1}^{n}\mathrm{d}\alpha_{ji}\right)\right]\times\cdots\right. \\ &\left.\exp\left(-\frac{1}{2}\sum_{i=1}^{N}\frac{\left[\bar{\boldsymbol{\alpha}}_{i+1}-\bar{\boldsymbol{\alpha}}_i-\Delta t\mathbf{A}(\bar{\boldsymbol{\alpha}}_i, t_i)\right]^{\mathrm{T}}\left[\tilde{\mathbf{B}}(\bar{\boldsymbol{\alpha}}_i, t_i)\right]^{-1}\left[\bar{\boldsymbol{\alpha}}_{i+1}-\bar{\boldsymbol{\alpha}}_i-\Delta t\mathbf{A}(\bar{\boldsymbol{\alpha}}_i, t_i)\right]}{\Delta t}\right)\right\} \\ &= \exp\left(-\int_{t_0}^{t_f}\mathcal{L}(\boldsymbol{\alpha}, \dot{\boldsymbol{\alpha}})\mathrm{d}t\right)\prod_{j=1}^{n}\prod_{t=t_0}^{t_f}\frac{\mathrm{d}\alpha_j(t)}{\sqrt{2\pi\left(\det\left[\tilde{\mathbf{B}}(\boldsymbol{\alpha}, t)\right]\right)^{\frac{1}{n}}\mathrm{d}t}} \end{aligned} \tag{9}$$

where

$$\mathcal{L}(\boldsymbol{\alpha}, \dot{\boldsymbol{\alpha}}) = \frac{1}{2}\left[\dot{\boldsymbol{\alpha}}-\mathbf{A}(\boldsymbol{\alpha}, t)\right]^{\mathrm{T}}\left[\tilde{\mathbf{B}}(\boldsymbol{\alpha}, t)\right]^{-1}\left[\dot{\boldsymbol{\alpha}}-\mathbf{A}(\boldsymbol{\alpha}, t)\right] \tag{10}$$

denotes the Lagrangian of the system. Further, the total probability that the process $\boldsymbol{\alpha}$ starts from $\boldsymbol{\alpha}_0$ at time t_0 and ends up at $\boldsymbol{\alpha}_f$ at t_f takes the form of a functional integral, which "sums up" the probabilities associated with each and every path that $\boldsymbol{\alpha}$ can possibly follow (e.g., [28]). In this regard, denoting by $\mathcal{C}\{\boldsymbol{\alpha}_0, t_0; \boldsymbol{\alpha}_f, t_f\}$ the set of all paths with initial state $\boldsymbol{\alpha}_0$ at time t_0 and final state $\boldsymbol{\alpha}_f$ at time t_f, the transition PDF takes the form

$$p(\boldsymbol{\alpha}_f, t_f|\boldsymbol{\alpha}_0, t_0) = \int_{\mathcal{C}\{\boldsymbol{\alpha}_0, t_0; \boldsymbol{\alpha}_f, t_f\}}\exp\left(-\int_{t_0}^{t_f}\mathcal{L}(\boldsymbol{\alpha}, \dot{\boldsymbol{\alpha}})\mathrm{d}t\right)\prod_{j=1}^{n}\mathcal{D}[\alpha_j(t)] \tag{11}$$

where

$$\mathcal{D}[\alpha_j(t)] = \prod_{t=t_0}^{t_f}\frac{\mathrm{d}\alpha_j(t)}{\sqrt{2\pi\left(\det\left[\tilde{\mathbf{B}}(\boldsymbol{\alpha}, t)\right]\right)^{\frac{1}{n}}\mathrm{d}t}} \tag{12}$$

is a functional measure.

3. Wiener path integral formalism for structural/mechanical dynamical systems

3.1. WPI Formulation

In this section, the formulation delineated in Section 2.2 is adapted to account for systems whose dynamics is governed by second-order SDEs; see also [4,6] for more details. Such cases include structural and/or mechanical dynamical systems with inertia terms in the respective equations of motion, which are generally modeled as a set of n coupled nonlinear second-order SDEs of the form

$$\mathbf{M}\ddot{\boldsymbol{x}} + \boldsymbol{g}(\boldsymbol{x}, \dot{\boldsymbol{x}}, t) = \boldsymbol{w}(t) \tag{13}$$

In Eq. (13), $\boldsymbol{x} = [x_j(t)]_{n\times 1}$ is the system response displacement vector; $\mathbf{M}$ represents the $n \times n$ mass matrix; $\boldsymbol{g} = [g_j(\boldsymbol{x}, \dot{\boldsymbol{x}}, t)]_{n\times 1}$ is an arbitrary nonlinear vector-valued function, which can account also for hysteretic response behaviors; and $\boldsymbol{w}$ is a white noise stochastic excitation vector process with $\mathbb{E}[\boldsymbol{w}(t)] = \mathbf{0}$ and $\mathbb{E}[\boldsymbol{w}(t)\boldsymbol{w}^{\mathrm{T}}(t-\tau)] = \mathbf{D}\delta(\tau)$, where $\mathbf{D} \in \mathbb{R}^{n\times n}$ is a deterministic coefficient matrix.

Next, introducing a new variable $\boldsymbol{v} = \dot{\boldsymbol{x}}$, Eq. (13) can be cast, equivalently, into the form of Eq. (1) with

$$\boldsymbol{\alpha} = \begin{bmatrix} \boldsymbol{x} \\ \boldsymbol{v} \end{bmatrix}, \quad \boldsymbol{A}(\boldsymbol{\alpha}, t) = \begin{bmatrix} \boldsymbol{v} \\ -\mathbf{M}^{-1}\boldsymbol{g}(\boldsymbol{x}, \boldsymbol{v}, t) \end{bmatrix} \quad \text{and}$$

$$\mathbf{B}(\boldsymbol{\alpha}, t) = \mathbf{B} = \begin{bmatrix} \mathbf{0} & \mathbf{0} \\ \mathbf{0} & \mathbf{M}^{-1}\sqrt{\mathbf{D}} \end{bmatrix} \tag{14}$$

where the square root of matrix $\mathbf{D}$ is given by $\sqrt{\mathbf{D}}\sqrt{\mathbf{D}}^{\mathrm{T}} = \mathbf{D}$. Clearly, the diffusion matrix $\tilde{\mathbf{B}} = \mathbf{B}\mathbf{B}^{\mathrm{T}}$ is singular (see Eq. (14)), and thus, the expression in Eq. (10) cannot be evaluated in a straightforward manner. Nevertheless, this limitation due to the singularity of $\tilde{\mathbf{B}}$ can be addressed by introducing delta-functionals to enforce the compatibility equation $\dot{\boldsymbol{x}} = \boldsymbol{v}$ (e.g., [6,28,29]). In particular, defining $\boldsymbol{S}(\boldsymbol{x}, \boldsymbol{v}, \dot{\boldsymbol{v}}) = \dot{\boldsymbol{v}} + \mathbf{M}^{-1}\boldsymbol{g}(\boldsymbol{x}, \boldsymbol{v}, t)$ the transition PDF of $\boldsymbol{\alpha}$ given by Eq. (11) becomes

$$p(\boldsymbol{\alpha}_f, t_f|\boldsymbol{\alpha}_0, t_0) = \int_{C\{\boldsymbol{x}_0,\boldsymbol{v}_0,t_0;\boldsymbol{x}_f,\boldsymbol{v}_f,t_f\}} \exp\left(-\int_{t_0}^{t_f} \frac{1}{2}\left[\mathbf{M}\boldsymbol{S}(\boldsymbol{x}, \boldsymbol{v}, \dot{\boldsymbol{v}})\right]^{\mathrm{T}}\mathbf{D}^{-1}\left[\mathbf{M}\boldsymbol{S}(\boldsymbol{x}, \boldsymbol{v}, \dot{\boldsymbol{v}})\right]\mathrm{d}t\right) \times \delta[\dot{\boldsymbol{x}} - \boldsymbol{v}]\, D[\boldsymbol{x}(t)]D[\boldsymbol{v}(t)] \tag{15}$$

For the derivation of Eq. (15), the relationship $\left(\mathbf{M}^{-1}\mathbf{D}\mathbf{M}^{-\mathrm{T}}\right)^{-1} = \mathbf{M}^{\mathrm{T}}\mathbf{D}^{-1}\mathbf{M}$ for an arbitrary non-singular square matrix $\mathbf{D}$ has been taken into account. Following integration over all paths $\boldsymbol{v}(t)$, and adopting for convenience in the ensuing analysis the notation $\boldsymbol{g}(\boldsymbol{x}, \dot{\boldsymbol{x}}, t) = \boldsymbol{g}(\boldsymbol{x}, \dot{\boldsymbol{x}})$, Eq. (15) becomes

$$p(\boldsymbol{x}_f, \dot{\boldsymbol{x}}_f, t_f|\boldsymbol{x}_0, \dot{\boldsymbol{x}}_0, t_0) = \int_{C\{\boldsymbol{x}_0,\dot{\boldsymbol{x}}_0,t_0;\boldsymbol{x}_f,\dot{\boldsymbol{x}}_f,t_f\}} \exp\left(-\int_{t_0}^{t_f} \mathcal{L}(\boldsymbol{x}, \dot{\boldsymbol{x}}, \ddot{\boldsymbol{x}})\mathrm{d}t\right) D[\boldsymbol{x}(t)] \tag{16}$$

where

$$\mathcal{L}(\boldsymbol{x}, \dot{\boldsymbol{x}}, \ddot{\boldsymbol{x}}) = \frac{1}{2}\left[\mathbf{M}\ddot{\boldsymbol{x}} + \boldsymbol{g}(\boldsymbol{x}, \dot{\boldsymbol{x}})\right]^{\mathrm{T}}\mathbf{D}^{-1}\left[\mathbf{M}\ddot{\boldsymbol{x}} + \boldsymbol{g}(\boldsymbol{x}, \dot{\boldsymbol{x}})\right] \tag{17}$$

and $D[\boldsymbol{x}(t)] = \prod_{j=1}^{n} D[x_j(t)]$. Note that the form of Eqs. (15)–(17) can accommodate also cases of singular mass matrices M. This may be the case, for instance, when considering hysteresis models (e.g., Bouc–Wen) that employ auxiliary additional state variables governed by first-order only equations (e.g., [34]). These first-order equations can be directly cast into the form of Eq. (1), whereas inversion pertains to the non-singular part of M only; see also Section 5.2.

Further, it is readily seen that the singularity of the diffusion matrix $\tilde{\mathbf{B}}$, encountered due to the state-variable reformulation of the second-order Eq. (13) into the first-order Eq. (14), has been addressed in a rather direct and straightforward manner by the introduction of the delta-functional. Specifically, owning to the simple form of the compatibility equation $\dot{\boldsymbol{x}} = \boldsymbol{v}$ between the original variable and the state variable, functional integration over the state variable $\boldsymbol{v}$ is performed in a direct (and rather trivial) manner. However, singular diffusion matrices $\tilde{\mathbf{B}}$ due to reasons other than state-variable reformulation (e.g., cases of systems with only some of their DOFs excited, hysteresis modeling via additional auxiliary state equations, energy harvesters with coupled electro-mechanical equations, etc.) are not amenable, in general, to a similar trivial treatment. This is due to the significantly more complex form of the corresponding (compatibility) equations related to the singularities, and thus, a direct functional integration is not possible. To address this challenge, the WPI-based solution technique is generalized and extended in Section 4 by relying on a constrained variational formulation that can account for arbitrary forms of (compatibility) equations related to singular diffusion matrices.

3.2. WPI solution treatment

3.2.1. Most probable path approximation

In this section, the basic aspects of a variational technique are presented, which is typically referred to in the theoretical physics literature as the semi-classical approximation [28,29,32,35,36]. The technique relies on the concept of the "most probable path" (also referred to as classical path) for providing an approximation of the WPI in Eq. (16). Specifically, the largest contribution to the functional integral of Eq. (16) comes from the trajectory $\boldsymbol{x}_c(t)$ for which the integral in the exponential, also known as stochastic action, is minimized (e.g., [28]). According to calculus of variations (e.g., [37,38]) this trajectory $\boldsymbol{x}_c(t)$ with fixed endpoints satisfies the extremality condition

$$\delta\int_{t_0}^{t_f} \mathcal{L}(\boldsymbol{x}, \dot{\boldsymbol{x}}, \ddot{\boldsymbol{x}})\mathrm{d}t = 0 \tag{18}$$

which leads to the Euler–Lagrange (E-L) equations

$$\frac{\partial\mathcal{L}}{\partial x_j} - \frac{\partial}{\partial t}\frac{\partial\mathcal{L}}{\partial\dot{x}_j} + \frac{\partial^2}{\partial t}\frac{\partial\mathcal{L}}{\partial\ddot{x}_j} = 0, \quad j = 1, \ldots, n \tag{19}$$

with the set of boundary conditions

$$\begin{matrix} x_j(t_0) = x_{j,0} & \dot{x}_j(t_0) = \dot{x}_{j,0} \\ x_j(t_f) = x_{j,f} & \dot{x}_j(t_f) = \dot{x}_{j,f} \end{matrix} \qquad j = 1, \ldots, n \tag{20}$$

Next, solving Eqs. (19)–(20) yields the n-dimensional most probable path, $\boldsymbol{x}_c(t)$, and thus, a single point of the system response transition PDF is determined as [4]

$$p(\boldsymbol{x}_f, \dot{\boldsymbol{x}}_f, t_f|\boldsymbol{x}_0, \dot{\boldsymbol{x}}_0, t_0) \approx C\ \exp\left(-\int_{t_0}^{t_f} \mathcal{L}(\boldsymbol{x}_c, \dot{\boldsymbol{x}}_c, \ddot{\boldsymbol{x}}_c)\mathrm{d}t\right) \tag{21}$$

where C is a normalization constant. It can be readily seen by comparing Eqs. (16) and (21) that in the approximation of Eq. (21) only one trajectory, i.e., the most probable path $\boldsymbol{x}_c(t)$, is considered in evaluating the path integral of Eq. (16). Regarding the degree of approximation associated with Eq. (21), direct comparisons of Eq. (21) with pertinent MCS data related to various engineering dynamical systems have demonstrated satisfactory accuracy (e.g., [5–9,17]).

3.2.2. Rayleigh-Ritz solution technique for the most probable path

In general, Eqs. (19)–(20) cannot be solved analytically for the most probable path. Therefore, resorting to numerical solution schemes for boundary value problems (BVPs) is often necessary. Indicatively, since $\boldsymbol{x}_c$ is the solution of the variational problem

$$\text{minimize} \quad \mathcal{J}(\boldsymbol{x}, \dot{\boldsymbol{x}}, \ddot{\boldsymbol{x}}) = \int_{t_0}^{t_f} \mathcal{L}(\boldsymbol{x}, \dot{\boldsymbol{x}}, \ddot{\boldsymbol{x}})\mathrm{d}t \tag{22}$$

or, in other words, an extremum for the functional $\mathcal{J}$, a direct functional minimization formulation can be employed in conjunction with

a standard Rayleigh-Ritz solution technique (see [5,39,40]). In this regard, $\boldsymbol{x}(t)$ is approximated by

$$\hat{\boldsymbol{x}}(t) = \boldsymbol{\psi}(t) + \mathbf{Z}\boldsymbol{h}(t) \approx \boldsymbol{x}(t) \tag{23}$$

The function $\boldsymbol{\psi}(t)$ is chosen so that it satisfies the boundary conditions, while the trial functions $\boldsymbol{h}(t) = [h_l(t)]_{L\times 1}$ should vanish at the boundaries, i.e., $\boldsymbol{h}(t_0) = \boldsymbol{h}(t_f) = \mathbf{0}$; $\mathbf{Z} \in \mathbb{R}^{n\times L}$ is a coefficient matrix and L is the chosen number of trial functions considered. Utilizing a vectorized form of $\mathbf{Z}$, Eq. (23) is cast, equivalently, as

$$\hat{\boldsymbol{x}}(t) = \boldsymbol{\psi}(t) + \mathbf{H}(t)\boldsymbol{z} \tag{24}$$

with

$$\boldsymbol{z} = \begin{bmatrix} Z_1^{\mathrm{T}} \\ Z_2^{\mathrm{T}} \\ \vdots \\ Z_L^{\mathrm{T}} \end{bmatrix} \in \mathbb{R}^{nL} \quad \text{and} \quad \mathbf{H}(t) = \begin{bmatrix} \boldsymbol{h}^{\mathrm{T}}(t) & \mathbf{0} & \dots & \mathbf{0} \\ \mathbf{0} & \boldsymbol{h}^{\mathrm{T}}(t) & \dots & \mathbf{0} \\ \vdots & \vdots & \ddots & \vdots \\ \mathbf{0} & \mathbf{0} & \dots & \boldsymbol{h}^{\mathrm{T}}(t) \end{bmatrix} \tag{25}$$

where Z_l denotes the lth row of matrix $\mathbf{Z}$ and $\mathbf{H}(t)$ is an $n \times nL$ time-dependent matrix. Clearly, there is a wide range of choices for functions $\boldsymbol{\psi}$ and $\boldsymbol{h}$. In the ensuing analysis, the Hermite interpolating polynomials

$$\psi_j(t) = \sum_{k=0}^{3} a_{j,k} t^k \tag{26}$$

are adopted, i.e., $\boldsymbol{\psi}(t) = [\psi_j(t)]_{n\times 1}$, where the $n \times 4$ coefficients $a_{j,k}$ are determined by the $n \times 4$ boundary conditions in Eq. (20). For the trial functions, the shifted Legendre polynomials given by the recursive formula

$$\ell_{q+1}(t) = \frac{2q+1}{q+1}\left(\frac{2t - t_0 - t_f}{t_f - t_0}\right)\ell_q(t) - \frac{q}{q+1}\ell_{q-1}(t), \quad q = 1, \dots, L-1 \tag{27}$$

are employed, which are orthogonal in the interval $[t_0, t_f]$, with $\ell_0(t) = 1$; and $\ell_1(t) = (2t - t_0 - t_f)/(t_f - t_0)$. The trial functions take the form

$$h_l(t) = (t - t_0)^2(t - t_f)^2\ell_l(t) \tag{28}$$

where the factor $(t - t_0)^2(t - t_f)^2$ multiplies the lth-order Legendre polynomial $\ell_l(t)$ to yield the lth trial function $h_l(t)$. Note that $h_l(t)$ is a polynomial of order $l + 4$ and vanishes at the boundaries. Clearly, each component $\hat{x}_j(t)$ of $\hat{\boldsymbol{x}}(t)$ in Eq. (23) is a polynomial of order up to $L + 4$ in t.

A practical advantage of the Rayleigh-Ritz solution technique is that the variational problem (functional minimization) of Eq. (22) degenerates to an ordinary minimization problem of a function that depends on a finite number of variables [38]. Specifically, the functional $\mathcal{J}$, dependent on the n functions $\boldsymbol{x}(t)$ (and their time derivatives), is cast in the form

$$J(\boldsymbol{z}) := \mathcal{J}(\hat{\boldsymbol{x}}, \dot{\hat{\boldsymbol{x}}}, \ddot{\hat{\boldsymbol{x}}}) \tag{29}$$

which depends on a finite number of nL coefficients $\boldsymbol{z}$. The corresponding optimization problem takes the form

$$\min_{\boldsymbol{z}} J(\boldsymbol{z}) \tag{30}$$

Further, the extremality condition in Eq. (18) is replaced by the first-order optimality condition

$$\nabla J(\boldsymbol{z}) = \mathbf{0} \tag{31}$$

which represents essentially a set of nL nonlinear algebraic equations that need to be solved numerically. Once the solution $\boldsymbol{z}^*$ of the optimization problem in Eq. (30) is obtained, the most probable path $\boldsymbol{x}_c$ is determined via Eq. (24). Obviously, there is a wide range of standard numerical optimization schemes to be employed for obtaining the solution $\boldsymbol{z}^*$. Indicatively, these range from gradient based techniques (e.g., [41]) to rather heuristic global optimization methods (e.g., [42,43]).

3.2.3. Computational efficiency aspects

Irrespective of whether the E-L Eqs. (19)–(20) are used or Eq. (31) is employed, solving the related deterministic BVP for given boundary conditions yields a single point of the joint response PDF via Eq. (21). According to a brute-force implementation of the WPI technique, for a given time instant t_f, an effective domain of values $(\boldsymbol{x}_f, \dot{\boldsymbol{x}}_f)$ is considered for the joint response PDF $p(\boldsymbol{x}_f, \dot{\boldsymbol{x}}_f, t_f|\boldsymbol{x}_0, \dot{\boldsymbol{x}}_0, t_0)$. Next, discretizing the effective domain using R points in each dimension, the joint response PDF values are obtained corresponding to the points of the mesh. Specifically, for an n-DOF system with $2n$ stochastic dimensions (n displacements and n velocities) the number of BVPs to be solved is R^{2n}. It is clear that the computational cost becomes prohibitive for relatively high-dimensional systems. However, efficient implementations, such as in [7], can be utilized in conjunction with the WPI technique. Specifically, employing a polynomial expansion for the joint response PDF yields a number of BVPs to be solved equal to the number of the expansion coefficients. This implementation has been shown to follow approximately a power-law function of the form $\sim (2n)^d/d!$ (where d is the degree of the polynomial), which, depending on the value of n, can be orders of magnitude smaller than R^{2n} [7]. Moreover, it has been recently shown in [8] that a compressive sampling treatment in conjunction with an appropriate optimization algorithm can further reduce drastically the required number of deterministic BVPs to be solved numerically.

4. Generalization of the Wiener path integral formulation to account for singular diffusion matrices: A constrained variational problem

4.1. WPI formulation accounting for singular diffusion matrices

In this section, the WPI solution technique delineated in Section 3 is extended to account for a general class of systems with singular diffusion matrices. In this regard, a novel WPI based variational formulation with constraints is developed. Specifically, consider in the following the general class of structural/mechanical systems whose governing equation of motion takes the form

$$\mathbf{M}\ddot{\boldsymbol{x}} + \boldsymbol{g}(\boldsymbol{x}, \dot{\boldsymbol{x}}) = \begin{bmatrix} \boldsymbol{w}(t) \\ \mathbf{0} \end{bmatrix} \tag{32}$$

where $\mathbf{M}$ is an $n \times n$, (potentially singular) mass matrix, and $\boldsymbol{g}$ is a nonlinear vector valued function. Indicative examples of engineering systems whose dynamics is described by Eq. (32) include, but are not limited to, structures subject to excitations applied to some (and not all) of their DOFs, hysteretic (e.g., Bouc–Wen) systems modeled via additional auxiliary state equations [34], and certain electromechanical energy harvesters [17]. Next, comparing Eqs. (13) and (32), it can be readily seen that the $\mathbf{D}$ matrix corresponding to the right-hand-side of Eq. (32), and defined as

$$\begin{aligned} \mathbf{D}\delta(\tau) &= \mathbb{E}\left[\begin{bmatrix} \boldsymbol{w}(t) \\ \mathbf{0} \end{bmatrix}\begin{bmatrix} \boldsymbol{w}^{\mathrm{T}}(t+\tau) & \mathbf{0} \end{bmatrix}\right] \\ &= \begin{bmatrix} \mathbb{E}\left[\boldsymbol{w}(t)\boldsymbol{w}^{\mathrm{T}}(t+\tau)\right] & \mathbf{0} \\ \mathbf{0} & \mathbf{0} \end{bmatrix} = \begin{bmatrix} \mathbf{D}_{rr} & \mathbf{0} \\ \mathbf{0} & \mathbf{0} \end{bmatrix}\delta(\tau) \end{aligned} \tag{33}$$

is singular, and thus, the Lagrangian of Eq. (17) cannot be determined in a straightforward manner. Note that the symbol $\mathbf{D}_{rr}$ is used to denote the non-singular square sub-matrix of $\mathbf{D}$.

In the ensuing analysis, the singularity of $\mathbf{D}$ is addressed by partitioning the system of Eq. (32) into two coupled subsystems: one that contains the equations corresponding to vector $\boldsymbol{w}$ on the right-hand-side of Eq. (32) and another referring to the equations that correspond to the zero entries on the right-hand-side of Eq. (32); this yields

$$\begin{bmatrix} \mathbf{M}_r\ddot{\boldsymbol{x}} + \boldsymbol{g}_r(\boldsymbol{x}, \dot{\boldsymbol{x}}) \\ \mathbf{M}_s\ddot{\boldsymbol{x}} + \boldsymbol{g}_s(\boldsymbol{x}, \dot{\boldsymbol{x}}) \end{bmatrix} = \begin{bmatrix} \boldsymbol{w}(t) \\ \mathbf{0} \end{bmatrix} \tag{34}$$

Note that the upper subsystem, hereinafter referred to as the r–system, constitutes an underdetermined system of $n - m$ SDEs and the lower

subsystem, hereinafter referred to as the $s-$system, represents an underdetermined system of m homogeneous ODEs. Clearly, matrix $\mathbf{M}_r \in \mathbb{R}^{(n-m)\times n}$ consists of the first $n-m$ rows of matrix $\mathbf{M}$, while $\mathbf{M}_s \in \mathbb{R}^{m\times n}$ consists of the last m rows of $\mathbf{M}$. Further, by recasting Eq. (32) into the form of Eq. (34), it can be argued that the motion of the dynamical system in Eq. (32) is governed by the $r-$system of equations constrained by the $s-$system of equations.

Next, defining $\boldsymbol{x}(t) = [\boldsymbol{x}_r(t) \quad \boldsymbol{x}_s(t)]^{\mathrm{T}}$, $\mathbf{M}_r = [\mathbf{M}_{rr} \quad \mathbf{M}_{rs}]$ and $\mathbf{M}_s = [\mathbf{M}_{sr} \quad \mathbf{M}_{ss}]$, where $\mathbf{M}_{rr}$, $\mathbf{M}_{rs}$, $\mathbf{M}_{sr}$ and $\mathbf{M}_{ss}$ are square matrices, and employing a δ-functional as in Section 3.1, the WPI for the system response PDF takes the form

$$p(\boldsymbol{\alpha}_f, t_f|\boldsymbol{\alpha}_0, t_0) = \int_{C\{\boldsymbol{\alpha}_f, t_f|\boldsymbol{\alpha}_0, t_0\}} \exp\left(-\int_{t_0}^{t_f} \frac{1}{2}\left[\boldsymbol{S}_r(\boldsymbol{\alpha}, \dot{\boldsymbol{\alpha}})\right]^{\mathrm{T}} \mathbf{D}_{rr}^{-1}\left[\boldsymbol{S}_r(\boldsymbol{\alpha}, \dot{\boldsymbol{\alpha}})\right] \mathrm{d}t\right) \times \delta\left[\boldsymbol{S}_s(\boldsymbol{\alpha}, \dot{\boldsymbol{\alpha}})\right] D[\boldsymbol{x}_r(t)] D[\boldsymbol{x}_s(t)] \tag{35}$$

where $\boldsymbol{\alpha} = [\boldsymbol{x}_r, \boldsymbol{x}_s, \dot{\boldsymbol{x}}_r, \dot{\boldsymbol{x}}_s]^{\mathrm{T}}$, while

$$\boldsymbol{S}_r(\boldsymbol{\alpha}, \dot{\boldsymbol{\alpha}}) = \mathbf{M}_{rr}\ddot{\boldsymbol{x}}_r + \mathbf{M}_{rs}\ddot{\boldsymbol{x}}_s + \boldsymbol{g}_r(\boldsymbol{\alpha}) \tag{36}$$

and

$$\boldsymbol{S}_s(\boldsymbol{\alpha}, \dot{\boldsymbol{\alpha}}) = \mathbf{M}_{sr}\ddot{\boldsymbol{x}}_r + \mathbf{M}_{ss}\ddot{\boldsymbol{x}}_s + \boldsymbol{g}_s(\boldsymbol{\alpha}) \tag{37}$$

Following a similar procedure as in Section 3.1, the aim is to integrate over paths $\boldsymbol{x}_s(t)$ and to obtain a path integral formulation involving $\boldsymbol{x}_r(t)$ only. However, this is not generally possible because the argument of the δ-functional in Eq. (35) is not merely a trivial compatibility relationship, as in Section 3.1, but a rather complex general function of $\boldsymbol{x}_s$. To address this challenge, the equation $\boldsymbol{S}_s(\boldsymbol{\alpha}, \dot{\boldsymbol{\alpha}}) = \mathbf{0}$ is enforced explicitly and takes the form of a constraint $\boldsymbol{\phi}(\boldsymbol{x}, \dot{\boldsymbol{x}}, \ddot{\boldsymbol{x}}) = \mathbf{0}$ given by

$$\boldsymbol{\phi}(\boldsymbol{x}, \dot{\boldsymbol{x}}, \ddot{\boldsymbol{x}}) = \mathbf{M}_s\ddot{\boldsymbol{x}} + \boldsymbol{g}_s(\boldsymbol{x}, \dot{\boldsymbol{x}}) \tag{38}$$

In this regard, the transition PDF can be expressed in the compact form

$$p(\boldsymbol{x}_f, \dot{\boldsymbol{x}}_f, t_f|\boldsymbol{x}_0, \dot{\boldsymbol{x}}_0, t_0) = \int_{C\{\boldsymbol{x}_0, \dot{\boldsymbol{x}}_0, t_0; \boldsymbol{x}_f, \dot{\boldsymbol{x}}_f, t_f|\boldsymbol{\phi}=\mathbf{0}\}} \exp\left(-\int_{t_0}^{t_f} \mathcal{L}_r(\boldsymbol{x}, \dot{\boldsymbol{x}}, \ddot{\boldsymbol{x}})\mathrm{d}t\right) D[\boldsymbol{x}(t)] \tag{39}$$

where

$$\mathcal{L}_r(\boldsymbol{x}, \dot{\boldsymbol{x}}, \ddot{\boldsymbol{x}}) = \frac{1}{2}[\mathbf{M}_r\ddot{\boldsymbol{x}} + \boldsymbol{g}_r(\boldsymbol{x}, \dot{\boldsymbol{x}})]^T \mathbf{D}_{rr}^{-1}[\mathbf{M}_r\ddot{\boldsymbol{x}} + \boldsymbol{g}_r(\boldsymbol{x}, \dot{\boldsymbol{x}})] \tag{40}$$

and $C\{\boldsymbol{x}_0, \dot{\boldsymbol{x}}_0, t_0; \boldsymbol{x}_f, \dot{\boldsymbol{x}}_f, t_f|\boldsymbol{\phi} = \mathbf{0}\}$ denotes the set of all paths, with initial state $(\boldsymbol{x}_0, \dot{\boldsymbol{x}}_0)$ at time t_0 and final state $(\boldsymbol{x}_f, \dot{\boldsymbol{x}}_f)$ at time t_f, which satisfy the constraint $\boldsymbol{\phi}(\boldsymbol{x}, \dot{\boldsymbol{x}}, \ddot{\boldsymbol{x}}) = \mathbf{0}$.

4.2. Constrained variational problem solution treatment

Following the WPI formulation of Section 4.1, determining the most probable path is pursued next by seeking for the solutions of the $r-$system that satisfy also the constraints of the $s-$ system. This leads to the formulation of a constrained variational problem for the determination of the most probable path $\boldsymbol{x}_c$, i.e.,

$$\text{minimize} \quad \mathcal{J}_r(\boldsymbol{x}, \dot{\boldsymbol{x}}, \ddot{\boldsymbol{x}}) = \int_{t_0}^{t_f} \mathcal{L}_r(\boldsymbol{x}, \dot{\boldsymbol{x}}, \ddot{\boldsymbol{x}})\mathrm{d}t \tag{41}$$

$$\text{subject to} \quad \boldsymbol{\phi}(\boldsymbol{x}, \dot{\boldsymbol{x}}, \ddot{\boldsymbol{x}}) = \mathbf{0} \tag{42}$$

where the Lagrangian $\mathcal{L}_r$ in Eq. (41) corresponds to the $r-$system only and is given by Eq. (40), and the constraint function $\boldsymbol{\phi}$ is given by Eq. (38).

Constrained variational problems of the form of Eqs. (41)–(42) can be solved by employing the general Lagrange multipliers approach (e.g., [44,45]). This leads to an unconstrained variational problem by considering the auxiliary Lagrangian $\mathcal{L}^*(\boldsymbol{x}, \dot{\boldsymbol{x}}, \ddot{\boldsymbol{x}}) = \mathcal{L}_r(\boldsymbol{x}, \dot{\boldsymbol{x}}, \ddot{\boldsymbol{x}}) + \boldsymbol{\lambda}(t)\boldsymbol{\phi}(\boldsymbol{x}, \dot{\boldsymbol{x}}, \ddot{\boldsymbol{x}})$. This unconstrained problem yields a system of n Euler–Lagrange equations, similar to the ones in Eq. (19)–(20), to be solved together with the m constraint functions in Eq. (42) for the n unknown functions $\boldsymbol{x}(t)$ and the m unknown Lagrange multiplier functions $\boldsymbol{\lambda}(t)$; see for instance [17]. In practice, however, the reformulation of this complex system of $n+m$ equations into an equivalent first-order system, as dictated by most numerical BVP solvers, requires multiple time differentiations of the constraint functions. As a result, the time derivatives of the constraints are fulfilled, but not the constraints themselves. This is a common limitation in several numerical solution methods for BVPs as highlighted in [46]. Therefore, in the ensuing analysis, attention is directed to a Rayleigh-Ritz solution approach for the determination of the most probable path.

Specifically, following Section 3.2.2, the polynomial expansion of Eq. (24) is utilized for the response vector $\boldsymbol{x}(t)$. This reduces the functional $\mathcal{J}_r(\boldsymbol{x}, \dot{\boldsymbol{x}}, \ddot{\boldsymbol{x}})$ of Eq. (41) to a function

$$J_r(\boldsymbol{z}) := \mathcal{J}_r(\hat{\boldsymbol{x}}, \dot{\hat{\boldsymbol{x}}}, \ddot{\hat{\boldsymbol{x}}}) \tag{43}$$

which depends on the vectorized expansion parameters $\boldsymbol{z} \in \mathbb{R}^p$, where $p = nL$. Further, by defining the functions

$$\hat{\boldsymbol{\phi}}(\boldsymbol{z}, t) := \boldsymbol{\phi}(\hat{\boldsymbol{x}}, \dot{\hat{\boldsymbol{x}}}, \ddot{\hat{\boldsymbol{x}}}) \tag{44}$$

the constraints in Eq. (42) are replaced by $\hat{\boldsymbol{\phi}}(\boldsymbol{z}, t) = \mathbf{0}$. The adoption of the Rayleigh-Ritz solution approach simplifies the constrained variational problem in Eq. (41)–(42) to an ordinary constrained optimization problem of the form

$$\min_{\boldsymbol{z}\in\mathbb{R}^p} \quad J_r(\boldsymbol{z}) \tag{45}$$

$$\text{subject to} \quad \hat{\boldsymbol{\phi}}(\boldsymbol{z}, t) = \mathbf{0} \quad \forall\, t \in [t_0, t_f] \tag{46}$$

and facilitates further its numerical treatment. Taking into account Eq. (24), the solution $\boldsymbol{z}^*$ to the above problem yields the most probable path in the form $\hat{\boldsymbol{x}}_c(t) = \boldsymbol{\psi}(t) + \mathbf{H}(t)\boldsymbol{z}^*$. Next, a single point of the system response transition PDF can be determined via the semi-classical approximation of Eq. (21) as

$$p(\boldsymbol{x}_f, \dot{\boldsymbol{x}}_f, t_f|\boldsymbol{x}_0, \dot{\boldsymbol{x}}_0, t_0) \approx C \ \exp\left(-\int_{t_0}^{t_f} \mathcal{L}_r(\hat{\boldsymbol{x}}_c, \dot{\hat{\boldsymbol{x}}}_c, \ddot{\hat{\boldsymbol{x}}}_c)\mathrm{d}t\right) \tag{47}$$

where C is a normalization constant.

4.3. Linear constraints

The special case of function $\boldsymbol{g}_s$ in Eq. (34) taking the linear form $\boldsymbol{g}_s(\boldsymbol{x}, \dot{\boldsymbol{x}}) = \mathbf{C}_s\dot{\boldsymbol{x}} + \mathbf{K}_s\boldsymbol{x}$, where $\mathbf{C}_s \in \mathbb{R}^{m\times n}$ and $\mathbf{K}_s \in \mathbb{R}^{m\times n}$, leads to linear constraint functions in Eq. (42). This considerable simplification facilitates a computationally efficient numerical treatment of the optimization problem of Eqs. (45)–(46). In particular, a solution is pursued by restricting the optimization within the space of solutions of Eq. (46) via a nullspace approach. Specifically, linearity of the constraint equations ensures that $\hat{\boldsymbol{\phi}}(\boldsymbol{z}, t)$ is a vector of m polynomial functions of t, each of degree $L+4$ (see Eqs. (23)–(25), (38) and (44)), with coefficients linear in the nL unknown expansion parameters $\boldsymbol{z}$. Setting these polynomial coefficients equal to zero yields a set of $m(L+4)$ linear equations with $p = nL$ unknown variables. Next, these equations are cast as a linear system of the form

$$\mathbf{F}\boldsymbol{z} = \mathbf{d} \tag{48}$$

where $\mathbf{F} \in \mathbb{R}^{s\times p}$, $\mathbf{d} \in \mathbb{R}^s$ and $s = m(L+4)$. Of course, for any well-posed constrained optimization problem, the number of independent constraints is smaller than the dimension of $\boldsymbol{z}$. For the herein concerned problem, this yields $m(L+4) < p$, which provides the lower bound $L > \frac{4m}{n-m}$ for the number L of trial functions used in the polynomial expansion. The system in Eq. (48) is underdetermined, while $\mathbf{F}$ may not have full row rank, i.e., $r_F \leq s$. It is now possible to restrict minimization of the objective function $J_r = J_r(\boldsymbol{z})$, where $\boldsymbol{z} \in \mathbb{R}^p$, to the set of solutions of Eq. (48) that lie on a lower dimensional space of dimension $p - r_F$. To elaborate further, note that the vector space

$U \subseteq \mathbb{R}^p$ of solutions of the system $\mathbf{F}\boldsymbol{z} = \mathbf{0}$, can be fully described with the aid of a basis $\mathbf{S} = [\boldsymbol{s}_1\ \boldsymbol{s}_2 \ldots\ \boldsymbol{s}_{p-r_F}]$ for the nullspace of $\mathbf{F}$ [47], where $\mathbf{S} \in \mathbb{R}^{p\times(p-r_F)}$. In this regard, any element $\boldsymbol{z} \in U$ can be represented by an element $\boldsymbol{v} \in V \subseteq \mathbb{R}^{p-r_F}$ as $\boldsymbol{z} = \mathbf{S}\boldsymbol{v}$, and the vector space $U_d \subseteq \mathbb{R}^p$ of solutions of $\mathbf{F}\boldsymbol{z} = \mathbf{d}$ can be obtained as an affine transformation of U [48]. More specifically, the solutions $\boldsymbol{z} \in U_d$ of Eq. (48) can be represented as

$$\boldsymbol{z} = \mathbf{S}\boldsymbol{v} + \boldsymbol{z}_p \tag{49}$$

where $\boldsymbol{z}_p$ is any particular solution of Eq. (48) [47,48]; see also [49]. This approach enables the corresponding constrained optimization problem

$$\min_{\boldsymbol{z}\in\mathbb{R}^p} J_r(\boldsymbol{z}) \quad \text{subject to} \quad \mathbf{F}\boldsymbol{z} = \mathbf{d} \tag{50}$$

of dimension p to be recast into a lower dimensional unconstrained problem of dimension $p - r_F$ as

$$\min_{\boldsymbol{v}\in\mathbb{R}^{p-r_F}} J_r(\mathbf{S}\boldsymbol{v} + \boldsymbol{z}_p) \tag{51}$$

Note that the minimizer $\boldsymbol{z}^*$ of Eq. (50) can be obtained by the minimizer $\boldsymbol{v}^*$ of Eq. (51) using the relationship in Eq. (49).

Further, it is worth highlighting the special case of a linear oscillator with non-singular diffusion matrix (unconstrained problem), where the most probable path can be derived in closed-form. Specifically, the linear oscillator yields a quadratic objective function in Eq. (29) that can be written as

$$J(\boldsymbol{z}) = \frac{1}{2}\boldsymbol{z}^{\mathrm{T}}\mathbf{Q}\boldsymbol{z} + \mathbf{b}^{\mathrm{T}}\boldsymbol{z} \tag{52}$$

where matrix $\mathbf{Q}$ and vector $\mathbf{b}$ can be calculated numerically (see Eqs. (17), (22), (24) and (29)). Given that $\mathbf{Q}$ is positive definite, $J(\boldsymbol{z})$ has the unique minimizer $\boldsymbol{z}^* = -\mathbf{Q}^{-1}\mathbf{b}$ and the most probable path can be determined in closed-form via Eq. (24). This result can be utilized in conjunction with the nullspace approach described earlier in this section, to determine the most probable path of a linear oscillator with singular diffusion matrix in closed-form as well. This is the case where the constraint function is linear ($\boldsymbol{g}_s(\boldsymbol{x}, \dot{\boldsymbol{x}}) = \mathbf{C}_s\dot{\boldsymbol{x}} + \mathbf{K}_s\boldsymbol{x}$) and function $\boldsymbol{g}_r$ in Eq. (34) is also linear, i.e., $\boldsymbol{g}_r(\boldsymbol{x}, \dot{\boldsymbol{x}}) = \mathbf{C}_r\dot{\boldsymbol{x}} + \mathbf{K}_r\boldsymbol{x}$, where $\mathbf{C}_r \in \mathbb{R}^{(n-m)\times n}$ and $\mathbf{K}_r \in \mathbb{R}^{(n-m)\times n}$, while the optimization problem of Eq. (51) takes the form

$$\min_{\boldsymbol{v}\in\mathbb{R}^{p-r_F}} \quad \frac{1}{2}[\mathbf{S}\boldsymbol{v} + \boldsymbol{z}_p]^{\mathrm{T}}\mathbf{Q}[\mathbf{S}\boldsymbol{v} + \boldsymbol{z}_p] + \mathbf{b}^{\mathrm{T}}[\mathbf{S}\boldsymbol{v} + \boldsymbol{z}_p] \tag{53}$$

Next, solving the problem in Eq. (53) with respect to $\boldsymbol{v}$ leads to the unique stationary point

$$\boldsymbol{v}^* = -(\mathbf{S}^{\mathrm{T}}\mathbf{Q}\mathbf{S})^{-1}[\boldsymbol{z}_p^{\mathrm{T}}\mathbf{Q}\mathbf{S} + \mathbf{b}^{\mathrm{T}}\mathbf{S}] \tag{54}$$

which, in conjunction with Eqs. (24) and (49), yields the following closed-form expression for the most probable path, i.e.,

$$\hat{\boldsymbol{x}}_c(t) = \boldsymbol{\psi}(t) + \mathbf{H}(t)\left[\mathbf{S}(\mathbf{S}^{\mathrm{T}}\mathbf{Q}\mathbf{S})^{-1}[\boldsymbol{z}_p^{\mathrm{T}}\mathbf{Q}\mathbf{S} + \mathbf{b}^{\mathrm{T}}\mathbf{S}] - \boldsymbol{z}_p\right] \tag{55}$$

4.4. Nonlinear constraints

In the more general case of arbitrary nonlinear constraints, it is possible to formulate an optimization problem with nonlinear equality constraints to be solved by an appropriate numerical technique, such as a Newton scheme in conjunction with a Lagrange multiplier approach for the enforcement of constraints. Specifically, a necessary and sufficient condition for Eq. (46) to hold is

$$\boldsymbol{\xi}(\boldsymbol{z}) := \sqrt{\int_{t_0}^{t_f} \hat{\boldsymbol{\phi}}^2(\boldsymbol{z}, t)\mathrm{d}t} = \mathbf{0} \tag{56}$$

where integration and square root are performed element-wise, and thus, the corresponding optimization problem can be formulated as

$$\min_{\boldsymbol{z}\in\mathbb{R}^p} J_r(\boldsymbol{z}) \quad \text{subject to} \quad \boldsymbol{\xi}(\boldsymbol{z}) = \mathbf{0} \tag{57}$$

Next, two typically utilized methods for the solution of nonlinear optimization problems with equality constraints of the form of Eq. (57) are presented.

4.4.1. Sequential Quadratic Programming (SQP)

The optimization problem with equality constraints in Eq. (57) can be solved by using a Lagrange multiplier approach and by employing the corresponding Karush-Kuhn–Tucker (KKT) conditions [41]. To this aim, the Lagrangian function L_M is defined as

$$L_M(\boldsymbol{z}, \boldsymbol{\lambda}) = J_r(\boldsymbol{z}) - \boldsymbol{\lambda}^{\mathrm{T}}\boldsymbol{\xi}(\boldsymbol{z}) \tag{58}$$

where $\boldsymbol{\lambda} \in \mathbb{R}^m$ is a vector of Lagrange multipliers, and the Jacobian of the constraints is denoted as

$$A(\boldsymbol{z})^{\mathrm{T}} = \left[\nabla\xi_1(\boldsymbol{z}), \nabla\xi_2(\boldsymbol{z}), \ldots, \nabla\xi_m(\boldsymbol{z})\right] \tag{59}$$

The first-order KKT conditions for the optimization problem with equality constraints in Eq. (57) take the form of an $n+m$ system of equations with $n+m$ unknowns $\boldsymbol{z}$ and $\boldsymbol{\lambda}$ as

$$F(\boldsymbol{z}, \boldsymbol{\lambda}) = \begin{bmatrix} \nabla J_r(\boldsymbol{z}) - A(\boldsymbol{z})^{\mathrm{T}}\boldsymbol{\lambda} \\ \boldsymbol{\xi}(\boldsymbol{z}) \end{bmatrix} = \mathbf{0} \tag{60}$$

while the Jacobian of Eq. (60) becomes

$$F'(\boldsymbol{z}, \boldsymbol{\lambda}) = \begin{bmatrix} \nabla^2_{\boldsymbol{z}\boldsymbol{z}} L_M(\boldsymbol{z}, \boldsymbol{\lambda}) & -A(\boldsymbol{z})^{\mathrm{T}} \\ A(\boldsymbol{z}) & 0 \end{bmatrix} \tag{61}$$

Next, a Newton scheme is utilized for the solution of the KKT system in Eq. (60). The corresponding Newton step at the kth iteration $(\boldsymbol{z}^k, \boldsymbol{\lambda}^k)$ takes the form

$$\begin{bmatrix} \boldsymbol{z}^{k+1} \\ \boldsymbol{\lambda}^{k+1} \end{bmatrix} = \begin{bmatrix} \boldsymbol{z}^k \\ \boldsymbol{\lambda}^k \end{bmatrix} + \begin{bmatrix} \boldsymbol{p}^k \\ \boldsymbol{p}^k_{\boldsymbol{\lambda}} \end{bmatrix} \tag{62}$$

where $\boldsymbol{p}^k$ and $\boldsymbol{p}^k_{\boldsymbol{\lambda}}$ are obtained by solving the Newton-KKT system

$$\begin{bmatrix} \nabla^2_{\boldsymbol{z}\boldsymbol{z}} L_M(\boldsymbol{z}^k, \boldsymbol{\lambda}^k) & -A(\boldsymbol{z}^k)^{\mathrm{T}} \\ A(\boldsymbol{z}^k) & 0 \end{bmatrix} \begin{bmatrix} \boldsymbol{p}^k \\ \boldsymbol{p}^k_{\boldsymbol{\lambda}} \end{bmatrix} = \begin{bmatrix} -\nabla J_r(\boldsymbol{z}^k) + A(\boldsymbol{z}^k)^{\mathrm{T}}\boldsymbol{\lambda}^k \\ -\boldsymbol{\xi}(\boldsymbol{z}^k) \end{bmatrix} \tag{63}$$

Solving the system in Eq. (63) and utilizing Eqs. (60) and (62), the update formulas for $\boldsymbol{\lambda}^{k+1}$ and $\boldsymbol{z}^{k+1}$ are given by

$$\boldsymbol{\lambda}^{k+1} = \left[A_k B_k^{-1} A_k^{\mathrm{T}}\right]^{-1}\left[-\boldsymbol{\xi}_k + A_k B_k^{-1} G_k\right] \tag{64}$$

$$\boldsymbol{p}^k = B_k^{-1}\left(A_k^{\mathrm{T}}\boldsymbol{\lambda}^{k+1} - G_k\right) \tag{65}$$

$$\boldsymbol{z}^{k+1} = \boldsymbol{z}^k + \alpha_k \boldsymbol{p}^k \tag{66}$$

where $A_k := A(\boldsymbol{z}^k) \in \mathbb{R}^{m\times p}$, $B_k := \nabla^2_{\boldsymbol{z}\boldsymbol{z}} L_M(\boldsymbol{z}^k, \boldsymbol{\lambda}^k) \in \mathbb{R}^{p\times p}$, $\boldsymbol{\xi}_k := \boldsymbol{\xi}(\boldsymbol{z}^k) \in \mathbb{R}^m$ and $G_k := \nabla J_r(\boldsymbol{z}^k) \in \mathbb{R}^p$.

In passing, it is noted that the above proposed Newton solution scheme for the KKT system of Eq. (60) can be identified as a Sequential Quadratic Programming (SQP) methodology, which is a broader class of optimization algorithms capable of treating both equality and inequality constraints [41]. Further, in Eq. (66), $\boldsymbol{p}^k$ is the step direction and α_k is a step size parameter that is equal to 1 in the standard implementation of the scheme (see Eq. (62)). In practice, however, a smaller value is typically chosen for the step size α_k as the iterations approach the local minimum. This yields faster convergence potentially, while the value of α_k at each iteration can be determined by an appropriate line search algorithm. In the following, a line search scheme based on Wolfe conditions and described in [50] is adopted in the numerical examples. Moreover, regarding numerical implementation of the optimization scheme, the standard Broyden–Fletcher–Goldfarb–Shanno (BFGS) formula [51,52] is employed herein for approximating the inverse of the Hessian matrix $\nabla^2_{\boldsymbol{z}\boldsymbol{z}} L_M$; see also [41] for a broader perspective.

4.4.2. Augmented Lagrangian Method (ALM)

A relatively popular alternative approach for the solution of the constrained optimization problem in Eq. (57) is the Augmented Lagrangian Method (ALM) [53–55]. The ALM approximates the solution

by successively minimizing the augmented Lagrangian function

$$L_A(\boldsymbol{z},\lambda;\mu) = J_r(\boldsymbol{z}) - \sum_{j=1}^{m}\lambda_j\xi_j(\boldsymbol{z}) + \frac{\mu}{2}\sum_{j=1}^{m}\xi_j^2(\boldsymbol{z}) \tag{67}$$

for a sequence of penalty factors μ with increasing values. Therefore, a sequence of unconstrained subproblems is formulated, where the solution of the previous problem is used as the initial guess for the next one, i.e.,

$$\boldsymbol{z}^{k+1} = \underset{\substack{\boldsymbol{z}\in\mathbb{R}^p \\ \boldsymbol{z}_{init}=\boldsymbol{z}^k}}{\arg\min}\, L_A(\boldsymbol{z},\lambda^k;\mu^k) \tag{68}$$

where the Lagrange multiplier vector $\lambda = [\lambda_j]_{m\times 1}$ at each step is given by the explicit estimate

$$\lambda^{k+1} = \lambda^k - \mu^k\xi(\boldsymbol{z}^k) \tag{69}$$

and $\boldsymbol{z}_{init}$ denotes the initial guess for the solution of the corresponding optimization problem. The ALM has shown to improve the ill-posedness of the quadratic penalty method (QPM), as it can approximate the solution of the original problem even with moderate values of the penalty factor μ [41]. Also, the augmented Lagrangian function in Eq. (67) can be derived as the dual of the corresponding quadratic penalty function of the QPM, as shown in [56].

5. Numerical examples

To assess the reliability of the herein developed technique for determining the response PDF of stochastically excited MDOF systems with singular diffusion matrices, two indicative examples are considered in this section. The first example pertains to a 2-DOF oscillator, where only one DOF is stochastically excited. It is shown that the special case of a linear oscillator under Kanai–Tajimi earthquake excitation, which yields a singular diffusion matrix, can also be cast in that form and treated under the same framework. The second example refers to a single-degree-of-freedom (SDOF) Bouc–Wen hysteretic oscillator, where hysteresis is modeled by introducing an additional auxiliary state equation. The WPI-based system response PDF estimates are compared with pertinent MCS data (10,000 realizations) for assessing the accuracy of the herein developed technique. In this regard, a standard fourth-order Runge–Kutta numerical integration scheme is employed for solving the governing equations of motion within the MCS context.

5.1. 2-DOF oscillator with only one DOF stochastically excited

The following 2-DOF oscillator with only one DOF stochastically excited is considered in the present example. Specifically, the equation of motion takes the form

$$\boldsymbol{M}\ddot{\boldsymbol{x}} + \boldsymbol{C}\dot{\boldsymbol{x}} + \boldsymbol{K}\boldsymbol{x} + \varepsilon\boldsymbol{g}_{nl}(\boldsymbol{x},\dot{\boldsymbol{x}}) = \begin{bmatrix} w(t) \\ 0 \end{bmatrix} \tag{70}$$

where

$$\mathbf{M} = \begin{bmatrix} 1 & 0 \\ 0 & 1 \end{bmatrix}, \quad \mathbf{C} = \begin{bmatrix} 0.2 & -0.1 \\ -0.1 & 0.1 \end{bmatrix}, \quad \mathbf{K} = \begin{bmatrix} 2 & -1 \\ -1 & 1 \end{bmatrix} \tag{71}$$

and $S_0 = 0.1$, whereas three different forms are considered next for the nonlinear function $\boldsymbol{g}(\boldsymbol{x},\dot{\boldsymbol{x}})$.

5.1.1. Linear oscillator with linear constraints

First, a linear version of the 2-DOF oscillator of Eq. (70) with $\varepsilon = 0$ is considered. The WPI technique in conjunction with the closed-form expression in Eq. (55) for the most probable path is utilized, and the joint response PDF $p(\boldsymbol{x},\dot{\boldsymbol{x}})$ is calculated for two indicative time instants $t = 2$ s and $t = 8$ s. The corresponding marginal response PDFs are shown in Fig. 1 demonstrating a high degree of accuracy based on comparisons with the exact solution obtained by numerically solving the related Lyapunov differential equation for the time-dependent response covariance matrix (see for instance [34]).

5.1.2. Linear oscillator under Kanai–Tajimi earthquake excitation

A widely utilized earthquake excitation model relates to the Kanai–Tajimi power spectrum introduced in [57,58] and further generalized in [59] and [60]. The rationale behind the Kanai–Tajimi modeling relates to approximating the bedrock acceleration as a white noise process filtered through the soil deposit, which is modeled as a SDOF oscillator, i.e.,

$$\ddot{y} + 2\zeta_g\omega_g\dot{y} + \omega_g^2 y = -w(t) \tag{72}$$

where y, $\dot{y}$ and $\ddot{y}$ are the ground displacement, velocity and acceleration, respectively, relative to the bedrock, while $w(t)$ is a white noise process with $\mathbb{E}[w(t)w(t-\tau)] = 2\pi S_0\delta(\tau)$. In Eq. (72), ζ_g is the damping ratio and ω_g is the natural frequency of the ground whose values are taken equal to $\zeta_g = 0.6$ and $\omega_g = 5\pi$ rad/s [60]. The absolute ground acceleration in this case can be expressed as

$$\ddot{x}_g(t) = \ddot{y}(t) + w(t) \tag{73}$$

characterized by the Kanai–Tajimi power spectrum

$$S_{\ddot{x}_g}(\omega) = S_0\frac{\omega_g^4 + 4\zeta_g^2\omega_g^2\omega^2}{(\omega_g^2-\omega^2)^2 + 4\zeta_g^2\omega_g^2\omega^2} \tag{74}$$

Next, the equation of motion of a linear SDOF oscillator, with mass m_0, damping coefficient c_0 and stiffness k_0, under Kanai–Tajimi earthquake excitation takes the form

$$m_0\ddot{x} + c_0\dot{x} + k_0 x = -m_0\ddot{x}_g(t) \tag{75}$$

Further, dividing Eq. (75) by m_0 and considering Eqs. (72) and (73), the overall system can be written in the form

$$\mathbf{M}\ddot{\boldsymbol{z}} + \mathbf{C}\dot{\boldsymbol{z}} + \mathbf{K}\boldsymbol{z} = \begin{bmatrix} -1 \\ -1 \end{bmatrix} w(t) \tag{76}$$

where

$$\boldsymbol{z} = \begin{bmatrix} x \\ y \end{bmatrix}, \quad \mathbf{M} = \begin{bmatrix} 1 & 1 \\ 0 & 1 \end{bmatrix}, \quad \mathbf{C} = \begin{bmatrix} c_0/m_0 & 0 \\ 0 & 2\zeta_g\omega_g \end{bmatrix} \quad \text{and} \quad \mathbf{K} = \begin{bmatrix} k_0/m_0 & 0 \\ 0 & \omega_g^2 \end{bmatrix} \tag{77}$$

Clearly, the white noise process $w(t)$ in Eq. (76) can be equivalently expressed as a sum of two independent white noise processes, i.e., $w(t) = w_1(t) + w_2(t)$. In this regard, Eq. (76) becomes

$$\mathbf{M}\ddot{\boldsymbol{z}} + \mathbf{C}\dot{\boldsymbol{z}} + \mathbf{K}\boldsymbol{z} = \begin{bmatrix} -1 & -1 \\ -1 & -1 \end{bmatrix}\begin{bmatrix} w_1(t) \\ w_2(t) \end{bmatrix} \tag{78}$$

and hence, Eq. (76) takes the form of Eq. (13) with $\boldsymbol{w}(t) = [w_1(t), w_2(t)]^{\mathrm{T}}$. It can be readily seen in Eq. (78) that the white noise vector process $[w_1(t), w_2(t)]^{\mathrm{T}}$ is multiplied by a rank-one matrix. Thus, matrix $\mathbf{D}$ in Eq. (14) is also rank-one (it has the value of 2 in all its entries) which leads to a singular diffusion matrix $\tilde{\mathbf{B}}$. Next, Eq. (78) can be multiplied by the non-singular transformation matrix

$$\mathbf{T} = \begin{bmatrix} 1 & 0 \\ -1 & 1 \end{bmatrix} \tag{79}$$

and written, alternatively, as

$$\mathbf{TM}\ddot{\boldsymbol{z}} + \mathbf{TC}\dot{\boldsymbol{z}} + \mathbf{TK}\boldsymbol{z} = \mathbf{T}\begin{bmatrix} -1 & -1 \\ -1 & -1 \end{bmatrix}\begin{bmatrix} w_1(t) \\ w_2(t) \end{bmatrix} = \begin{bmatrix} -1 & -1 \\ 0 & 0 \end{bmatrix}\begin{bmatrix} w_1(t) \\ w_2(t) \end{bmatrix} = \begin{bmatrix} -w(t) \\ 0 \end{bmatrix} \tag{80}$$

Note that Eq. (80) has exactly the form of Eq. (70) with $\varepsilon = 0$, and thus, can be treated by the herein developed technique. Further, since Eq. (80) is linear, the solution approach of Section 4.3 can be applied, where the most probable path is given by Eq. (55) in closed form. The corresponding marginal response PDFs are shown in Fig. 2 for an oscillator with parameters $m_0 = 1$, $c_0 = 0.2$, $k_0 = 1$ and $S_0 = 0.5$. Comparisons with MCS data obtained by utilizing the spectral representation method [61] to generate realizations compatible with the

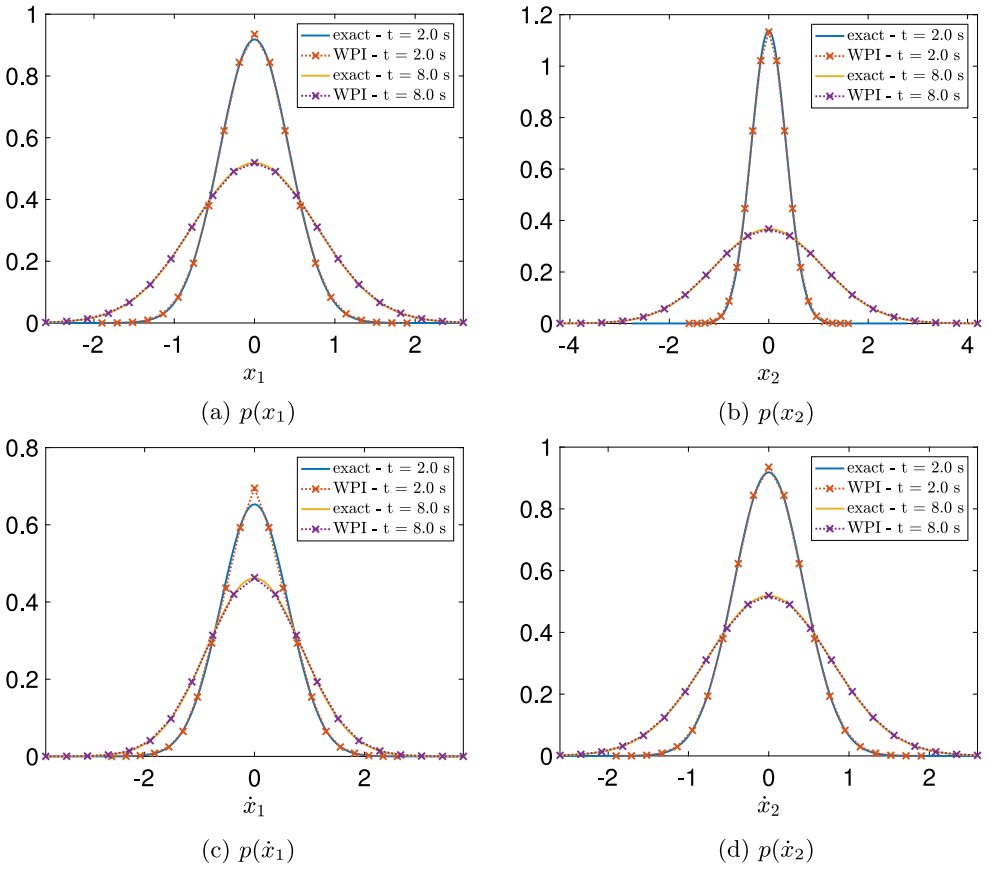

(a) $p(x_1)$ (b) $p(x_2)$ (c) $p(\dot{x}_1)$ (d) $p(\dot{x}_2)$

Fig. 1. Marginal response PDFs of a stochastically excited 2-DOF linear oscillator with linear constraints; comparisons with exact solutions.

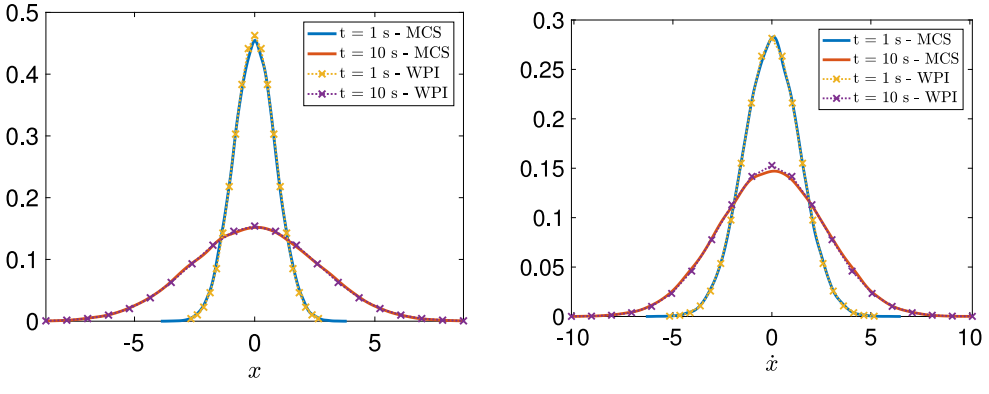

(a) $p(x)$ (b) $p(\dot{x})$

Fig. 2. Marginal response PDFs of a SDOF linear oscillator under Kanai–Tajimi earthquake excitation; comparisons with MCS data (10,000 realizations).

Kanai–Tajimi power spectrum of Eq. (74) demonstrate a high degree of accuracy.

5.1.3. Nonlinear oscillator with linear constraints

Next, a version of the 2-DOF oscillator of Eq. (70) with stiffness and damping nonlinearities in the first equation and linear second equation is considered; thus, yielding linear constraints in the herein developed computational framework. In particular, the nonlinear function $\boldsymbol{g}_{nl}(\boldsymbol{x}, \dot{\boldsymbol{x}})$ takes the form

$$\boldsymbol{g}_{nl}(\boldsymbol{x}, \dot{\boldsymbol{x}}) = \begin{bmatrix} c_{11}\dot{x}_1^3 + k_{11}x_1^3 \\ 0 \end{bmatrix} \tag{81}$$

where x_1 is the first component of the response vector $\boldsymbol{x}$, c_{11} and k_{11} are the upper left elements of matrices $\mathbf{C}$ and $\mathbf{K}$, respectively, and the magnitude of the nonlinearity ϵ is taken equal to 0.5.

The WPI technique in conjunction with the methodology described in Section 4.3 is utilized next, and the joint response PDF $p(\boldsymbol{x}, \dot{\boldsymbol{x}})$ is calculated for two indicative time instants $t = 2$ s and $t = 8$ s. The corresponding marginal response PDFs are presented in Fig. 3, and compared with pertinent MCS data (10,000 realizations). The accuracy degree exhibited by the WPI is generally high, whereas slight deviations from the MCS-based estimates, such as in Fig. 3(c), may be attributed not only to the various approximations involved in the WPI technique (see Section 3), but also to the specific accuracy characterizing the MCS-based estimate given the utilized number of realizations.

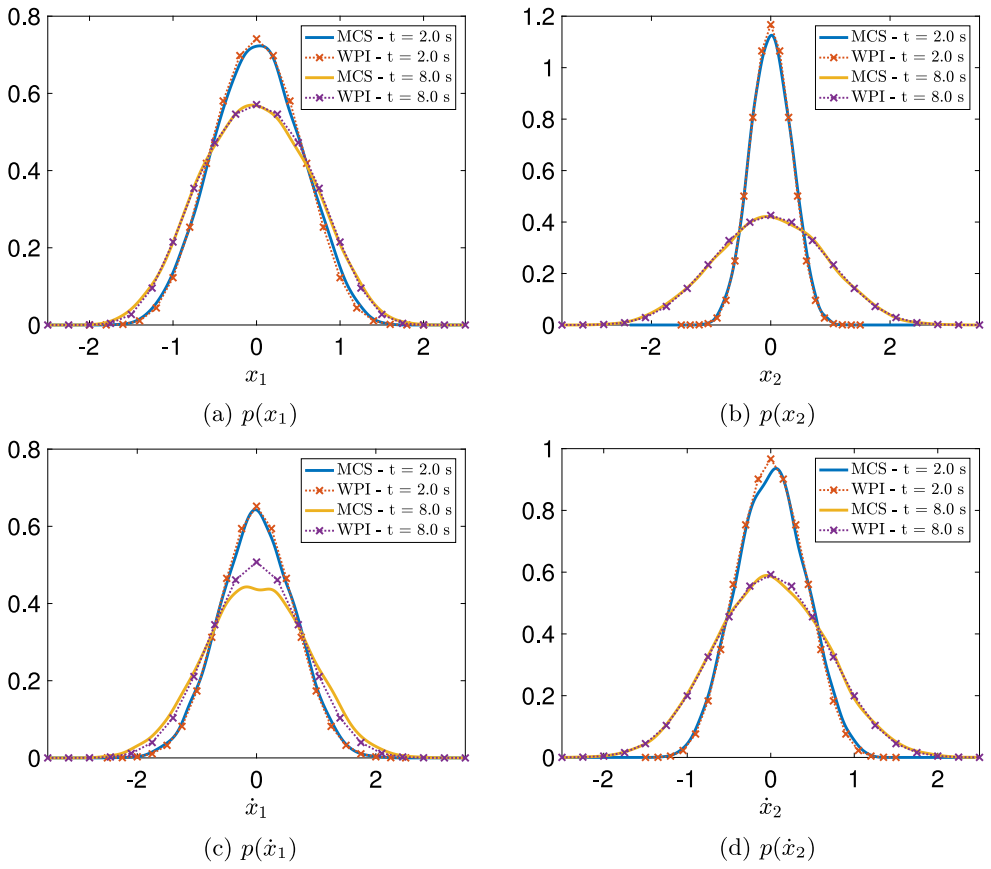

Fig. 3. Marginal response PDFs of a stochastically excited 2-DOF nonlinear oscillator with linear constraints; comparisons with MCS data (10,000 realizations).

5.1.4. Nonlinear oscillator with nonlinear constraints

Further, a third version of the 2-DOF oscillator in Eq. (70) with stiffness nonlinearities in both equations is considered; thus, yielding nonlinear constraints in the proposed computational framework. In this case, the nonlinear function $\boldsymbol{g}_{nl}(\boldsymbol{x}, \dot{\boldsymbol{x}})$ takes the form

$$\boldsymbol{g}_{nl}(\boldsymbol{x}, \dot{\boldsymbol{x}}) = \begin{bmatrix} k_{11}x_1^3 \\ k_{22}x_2^3 \end{bmatrix} \tag{82}$$

where x_1 and x_2 are the first and second components of the response vector $\boldsymbol{x}$, k_{11} and k_{22} are the upper left and lower right elements of matrix $\mathbf{K}$, respectively, and the nonlinearity magnitude ϵ is taken equal to 0.5.

The WPI technique in conjunction with the SQP method described in Section 4.4.1 is utilized next. In this regard, each point of the joint response PDF $p(\boldsymbol{x}, \dot{\boldsymbol{x}})$ at time $t = 1$ s is obtained as described in Section 3.2.3 by utilizing the SQP algorithm combined with a line search scheme and by employing the BFGS formula, with an initial guess $\boldsymbol{z}_{init} = \mathbf{0}$. Following integration of the joint response PDF, the corresponding marginal PDFs are obtained and presented in Fig. 4. Comparisons with pertinent MCS data (10,000 realizations) demonstrate a high degree of accuracy.

Further, the joint response PDFs $p(x_1, x_2)$, $p(x_1, \dot{x}_1)$ and $p(x_2, \dot{x}_2)$ are also shown in Figs 5, 6 and 7, respectively, for the two time instants $t = 1$ s and $t = 3$ s. In a similar manner as before, satisfactory accuracy is observed based on comparisons with corresponding MCS data.

Next, the WPI technique in conjunction with the ALM method described in Section 4.4.2 is utilized. In this context, each point of the joint response PDF $p(\boldsymbol{x}, \dot{\boldsymbol{x}})$ at time $t = 1$ s is obtained by successively minimizing the augmented Lagrangian function of Eq. (67), for the sequence of penalty factors with increasing values $\mu = 3^k$ for $k = 0$, 2, 4, 6, 8, 10, 12. Following integration of the joint response PDF, the corresponding marginal PDFs are obtained for three indicative values of μ and presented in Fig. 8. A comparison with pertinent MCS results (10,000 realizations) shows the convergence of the marginal PDFs to the MCS-based estimates for increasing values of μ.

It is seen that both the SQP and the ALM optimization schemes of sections 4.4.1 and 4.4.2, respectively, perform satisfactorily in solving the problem of Eq. (57) with relatively high accuracy. Nevertheless, there are cases where the SQP algorithm may not converge to the optimum value for various reasons, such as poor choice of the initial guess or non-smooth and numerically ill-behaved governing/constraint equations. In such cases, the ALM or an appropriate combination of the SQP and ALM schemes may yield a more robust and efficient solution approach. An indicative example is considered next.

5.2. Bouc–Wen hysteretic oscillator

A SDOF Bouc–Wen nonlinear oscillator, which has been widely utilized in engineering dynamics for modeling systems exhibiting hysteresis, is considered in this numerical example. The introduction of the smooth and versatile Bouc–Wen hysteretic model [62,63] was followed by its successful application to various engineering mechanics related fields. Besides its versatility in efficiently capturing a broad range of hysteretic behaviors, corresponding equivalent linear elements can be readily determined in an explicit manner [64]. Specifically, a statistical linearization method (e.g., [34]) was proposed in [65] that involved deriving closed-form expressions for the equivalent linear elements of the Bouc–Wen model. Furthermore, a wavelet-based statistical linearization method was developed in [66] to determine the response evolutionary power spectrum. Indicatively, the Bouc–Wen formalism and its variants have been employed recently for modeling the inelastic behavior of steel beams with hysteretic damping [67], while in [68] a Bouc–Wen model compatible with plasticity postulates has been developed. A detailed presentation of the applications and the

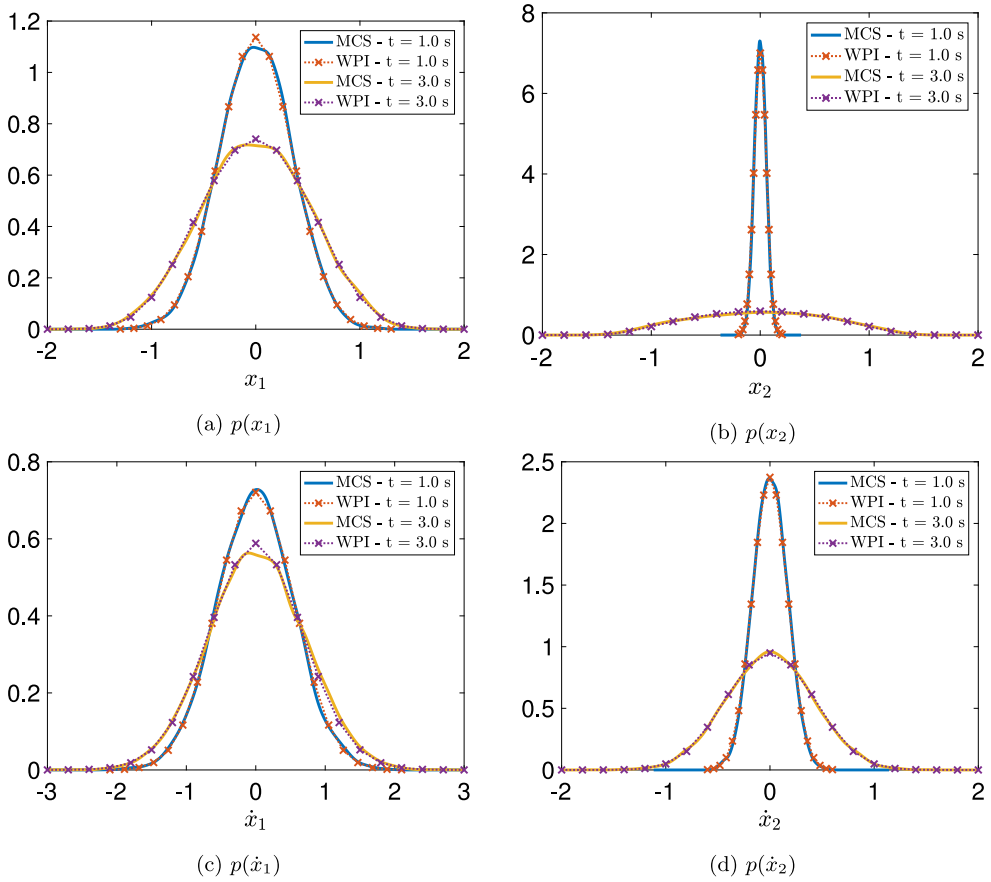

Fig. 4. Marginal response PDFs of a stochastically excited 2-DOF nonlinear oscillator with nonlinear constraints at $t = 1$ s and $t = 3$ s; comparisons with MCS data (10,000 realizations).

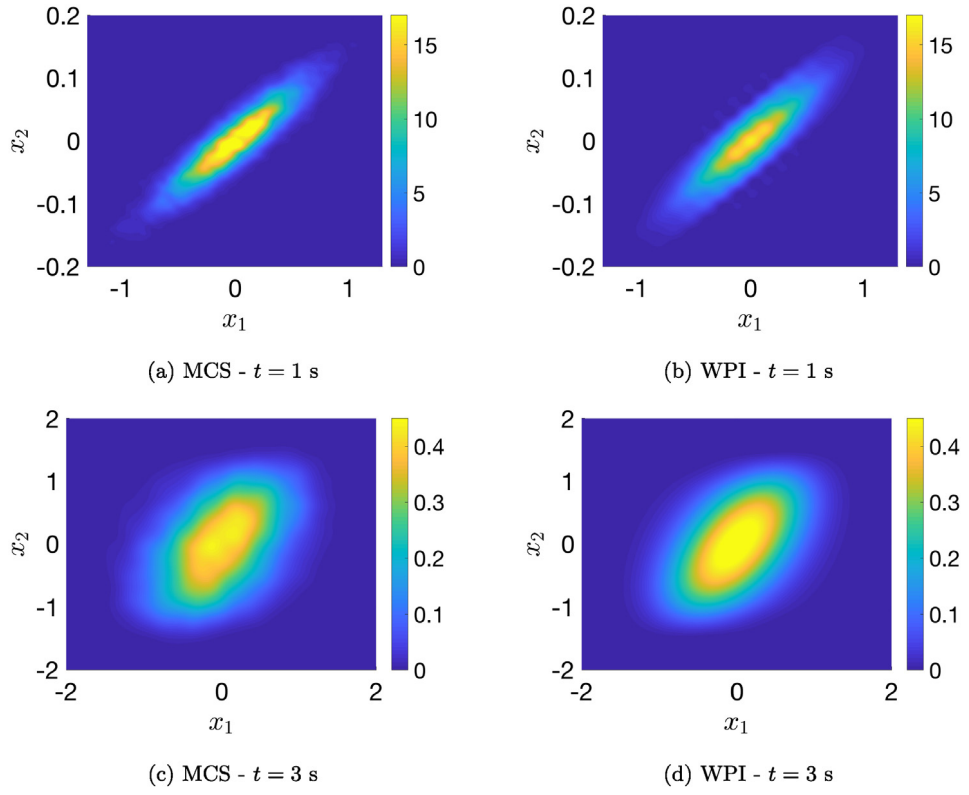

Fig. 5. Joint response PDF $p(x_1, x_2)$ of a stochastically excited 2-DOF nonlinear oscillator with nonlinear constraints at $t = 1$ s and $t = 3$ s.

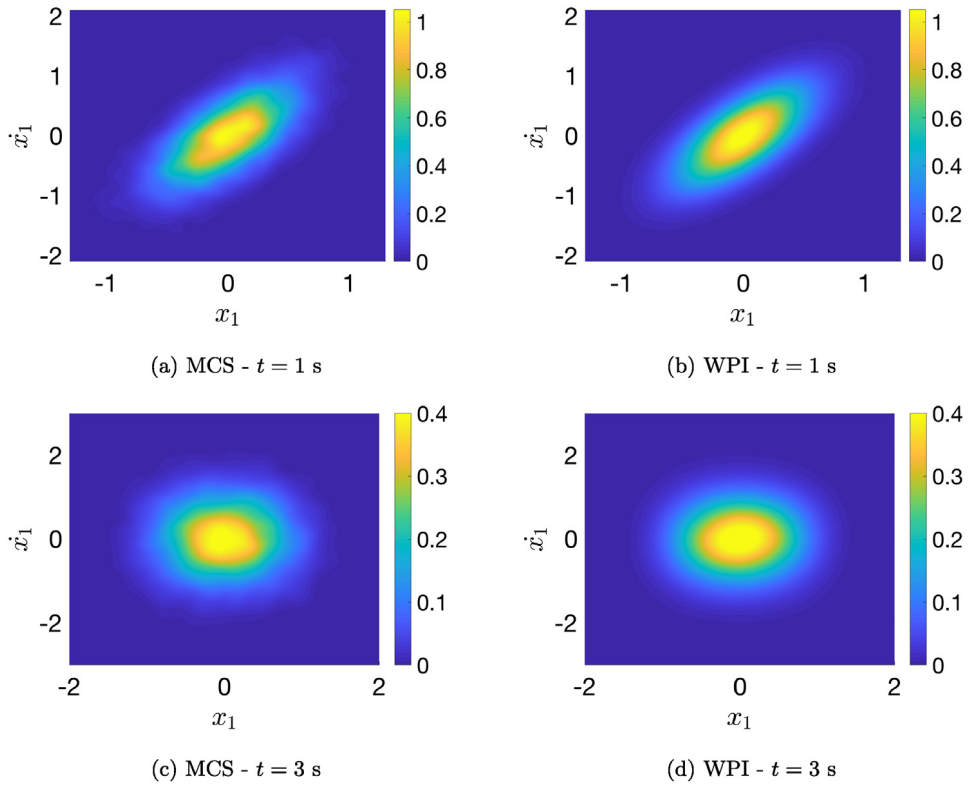

Fig. 6. Joint response PDF $p(x_1, \dot{x}_1)$ of a stochastically excited 2-DOF nonlinear oscillator with nonlinear constraints at $t = 1$ s and $t = 3$ s.

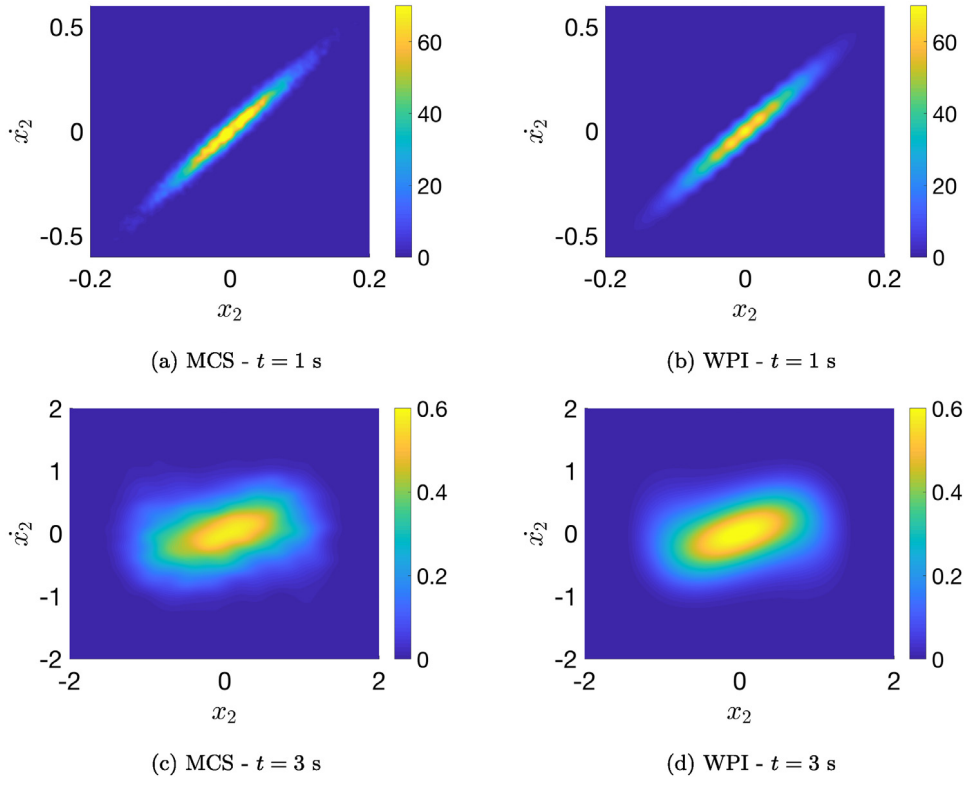

Fig. 7. Joint response PDF $p(x_2, \dot{x}_2)$ of a stochastically excited 2-DOF nonlinear oscillator with nonlinear constraints at $t = 1$ s and $t = 3$ s.

extensions of the Bouc–Wen model can be found in [16] and in review papers such as [69] and [70].

The Bouc–Wen oscillator is generally described by the system of coupled differential equations

$$\ddot{x} + 2\zeta_0\omega_0\dot{x} + \alpha\omega_0^2 x + (1-\alpha)\omega_0^2 z = w(t) \tag{83}$$

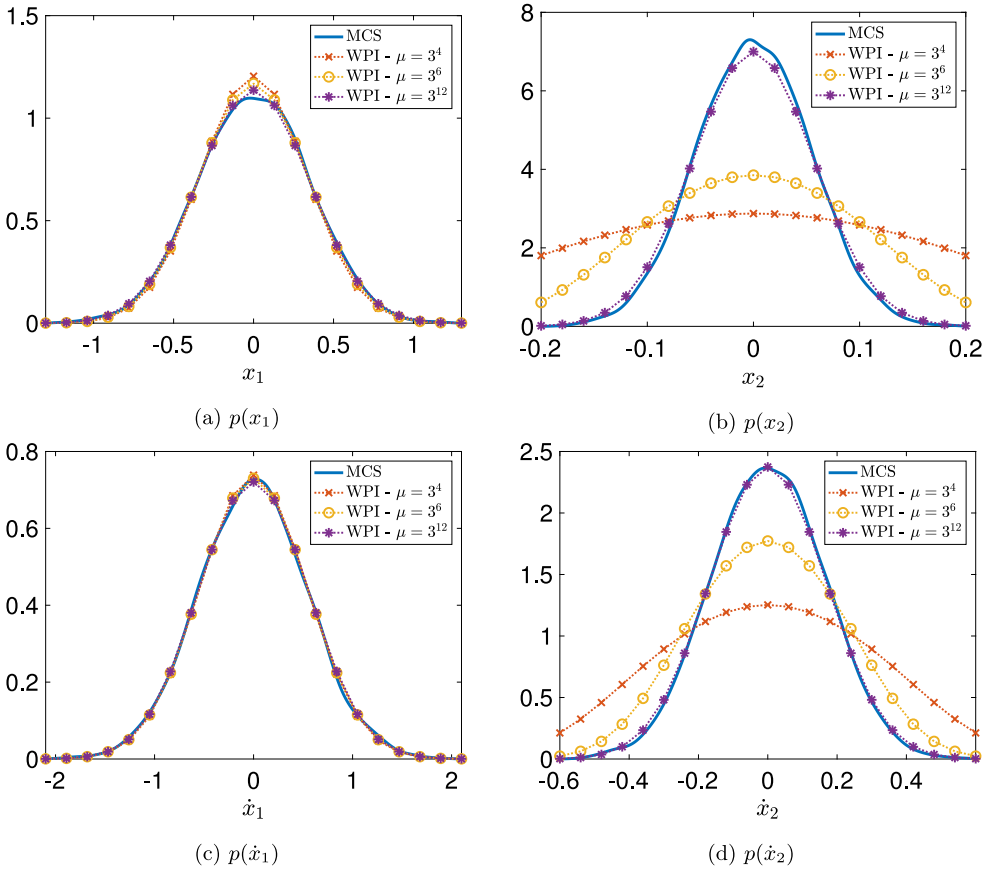

(a) $p(x_1)$ (b) $p(x_2)$

(c) $p(\dot{x}_1)$ (d) $p(\dot{x}_2)$

Fig. 8. Marginal response PDFs of a stochastically excited 2-DOF nonlinear oscillator with nonlinear constraints at $t = 1$ s for increasing values of the penalty factor μ; comparisons with MCS data (10,000 realizations).

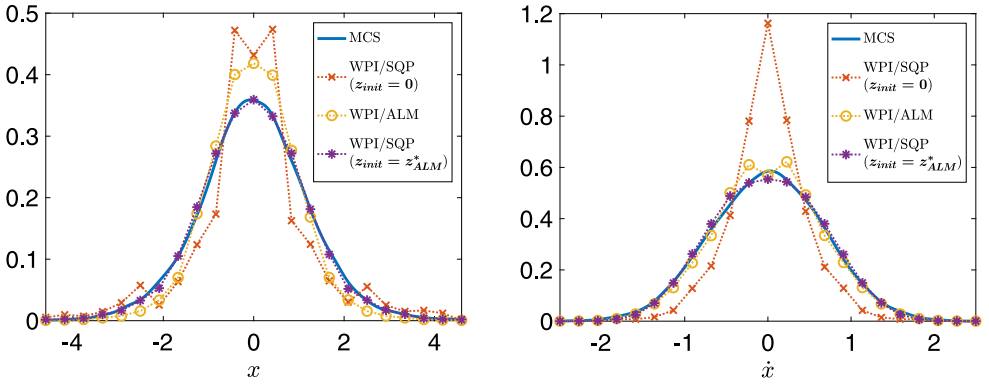

(a) $p(x)$ (b) $p(\dot{x})$

Fig. 9. Marginal response PDFs of a SDOF Bouc–Wen oscillator at $t = 10$ s by employing various optimization schemes; comparisons with pertinent MCS data (10,000 realizations).

$$\dot{z} + \gamma|\dot{x}|z|z|^{\nu-1} + \beta\dot{x}|z|^{\nu} - A\dot{x} = 0 \tag{84}$$

where in Eq. (83) α can be viewed as a form of post-yield-to-pre-yield stiffness ratio. In the Bouc–Wen model, the additional auxiliary state z is related to the response x via Eq. (84). Various both softening and hardening behaviors can be modeled by appropriately choosing the constant parameters γ, β and A (see e.g., [70]).

Clearly, Eqs. (83)–(84) can be construed as a coupled system of a SDE (Eq. (83)) and a homogeneous ODE (Eq. (84)). This can be readily cast in the form of Eq. (32), and thus, treated by the herein developed solution technique. In passing, it is worth mentioning that, due to Eq. (84) being first-order, the system augmented mass matrix $\mathbf{M}$ in Eq. (13) is singular. Nevertheless, this poses no difficulties in applying the solution technique in a rather straightforward manner; see also discussion following Eq. (17). Moreover, it is noted that the Bouc–Wen model in Eqs. (83) and (84) has some special characteristics that affect the form of the corresponding optimization problem. In particular, Eq. (83) is linear, which yields a corresponding objective function of a quadratic form (see Eq. (52)). This suggests that the SQP method presented in Section 4.4.1 is expected to perform satisfactorily, as it is essentially a quasi-Newton method. However, due to the form of Eq. (84) containing multiplicative relations involving absolute value functions, the constraint function takes a relatively complex form that can be locally non-differentiable; thus, leading to a potentially ill-posed optimization problem.

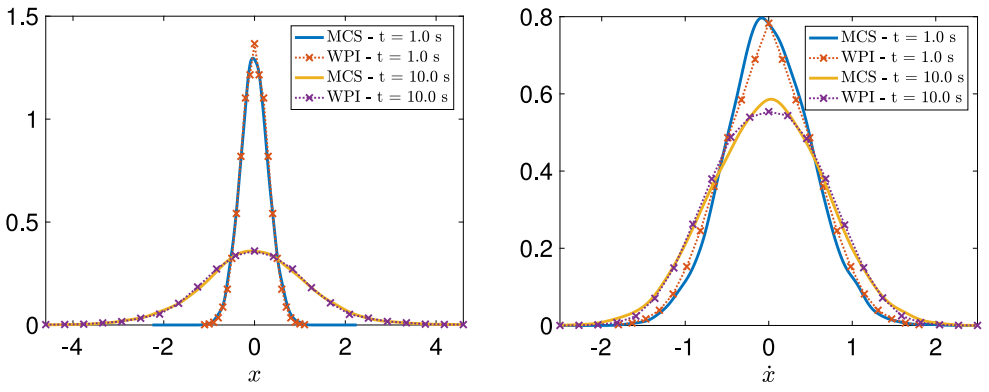

(a) $p(x)$ (b) $p(\dot{x})$

Fig. 10. Marginal response PDFs of a SDOF Bouc–Wen oscillator determined by the combined ALM/SQP approach at $t = 1$ s and $t = 10$ s.

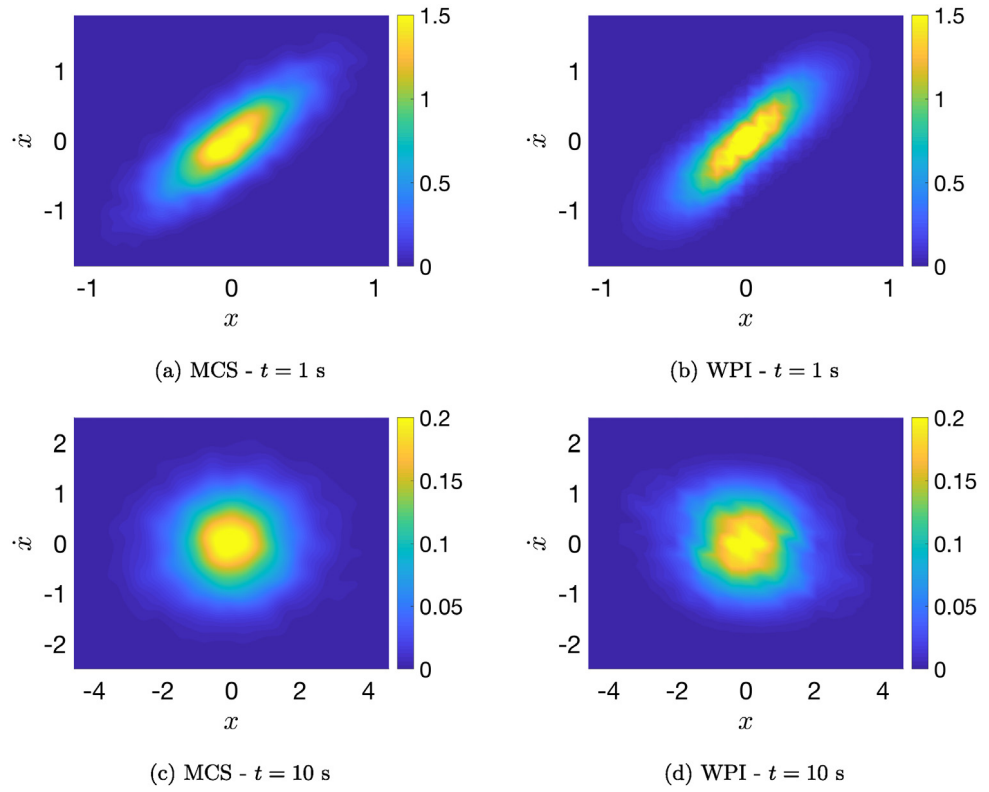

(a) MCS - $t = 1$ s (b) WPI - $t = 1$ s

(c) MCS - $t = 10$ s (d) WPI - $t = 10$ s

Fig. 11. Joint response PDF $p(x, \dot{x})$ of a SDOF Bouc–Wen oscillator determined by the combined ALM/SQP approach at $t = 1$ s and $t = 10$ s.

Next, for the parameter values $\zeta_0 = 0.01$, $\omega_0 = 1$, $\alpha = 0.01$, $\gamma = 0.5$, $\nu = 1$, $\beta = 0.5$ and $A = 1$, the joint response PDF $p(x, z, \dot{x})$ is obtained by employing the SQP method of Section 4.4.1 with an initial guess $\boldsymbol{z}_{init} = \mathbf{0}$. The corresponding marginal PDFs of the response displacement x and velocity $\dot{x}$ are plotted in Fig. 9 (line with x markers) for an indicative time instant $t = 10$ s. Clearly, based on comparisons with pertinent MCS data, this solution approach does not exhibit a satisfactory accuracy degree. As explained earlier, this may be due to a potentially ill-posed optimization problem, or due to the initial guess $\boldsymbol{z}_{init}$ not being sufficiently close to the optimum. In this regard, it can be argued that an ALM solution treatment may be, perhaps, a more appropriate choice. Specifically, for a sequence of penalty factors starting from zero, the initial ALM optimization problem becomes unconstrained and convex (quadratic form); thus, yielding a unique solution. Next, given that the sequence of penalty factors is sufficiently long and densely discretized, the ALM solution approach could potentially converge to the global optimum, at the expense, however, of considerable computational cost due to the large number of optimization subproblems; see Eq. (68).

In this regard, an alternative hybrid solution approach is proposed, which attempts to benefit from the advantages of both the ALM and the SQP schemes. Specifically, an ALM run is performed first by using a small number of penalty factors with moderate values and by setting large convergence tolerances to accelerate convergence. Of course, this ALM step is not expected to yield the optimum with high accuracy (see line with o markers in Fig. 9). Instead, it is aimed to be used as a reasonable initial guess for the SQP methodology, which can now converge to a solution of relatively high accuracy (see line with * markers in Fig. 9) as compared to corresponding MCS data (10,000 realizations). Further, in Fig. 10 the marginal PDFs $p(x)$ and $p(\dot{x})$ are plotted for two indicative time instants as obtained by the above proposed hybrid ALM/SQP solution approach. In a similar manner as in Fig. 9, comparisons with relevant MCS data (10,000 realizations) show

a relatively high degree of accuracy exhibited by the WPI technique. Indeed, despite the non-smooth character of the nonlinearities involved in the Bouc–Wen model (e.g., absolute value functions in Eq. (84)) that render the problem rather challenging, the herein developed technique has performed satisfactorily in determining the response statistics. The corresponding joint response PDF $p(x, \dot{x})$ is shown in Fig. 11.

6. Concluding remarks

A methodology based on the WPI has been developed for determining the joint response transition PDF of a broad class of nonlinear dynamical systems with singular diffusion matrices. In this regard, the WPI technique has been extended herein to account for systems that can be represented, generally, as an underdetermined system of SDEs coupled with a set of ODEs. Indicative examples include (but are not limited to) systems with only some of the DOFs excited, hysteresis modeling via additional auxiliary state equations, and energy harvesters with coupled electro-mechanical equations. Next, interpreting the set of ODEs as constraint equations leads to a constrained variational problem to be solved for the most probable path, and thus, the joint response PDF is determined. To this aim, a direct functional minimization formulation has been applied, coupled with a standard Rayleigh-Ritz solution approach. This has reduced the constrained variational problem to an ordinary constrained optimization problem. It has been shown that a nullspace solution approach appears computationally efficient for cases of linear constraints, whereas a SQP scheme has been employed for the general case of nonlinear constraints. Further, a herein proposed hybrid ALM/SQP solution approach appears more appropriate for cases of non-smooth and numerically ill-behaved nonlinear constraint equations. In this paper, the reliability of the technique has been demonstrated by considering diverse numerical examples, including various 2-DOF oscillators with only one DOF excited. Interestingly, it has been shown that the special case of a linear oscillator under Kanai–Tajimi earthquake excitation, which yields a singular diffusion matrix, can also be cast in the aforementioned form and treated under the same framework. Further, the SDOF Bouc–Wen nonlinear hysteretic oscillator has also been considered. Comparisons with pertinent MCS data have demonstrated a relatively high degree of accuracy.

Acknowledgments

I. A. Kougioumtzoglou gratefully acknowledges the support through his CAREER award by the CMMI Division of the National Science Foundation, USA (Award number: 1748537). The authors acknowledge the interaction with Professor Kostas Papakonstantinou and his useful insight during the early stages of the paper.

References

[1] M. Grigoriu, Stochastic Calculus: Applications in Science and Engineering, Birkhäuser, Boston-Basel-Baein, 2002.
[2] S.-K. Au, Y. Wang, Engineering Risk Assessment with Subset Simulation, John Wiley & Sons, New York, 2014.
[3] I. Kougioumtzoglou, P. Spanos, An analytical Wiener path integral technique for non-stationary response determination of nonlinear oscillators, Probab. Eng. Mech. 28 (2012) 125–131.
[4] I.A. Kougioumtzoglou, P.D. Spanos, Nonstationary stochastic response determination of nonlinear systems: A Wiener path integral formalism, J. Eng. Mech. 140 (9) (2014) 04014064.
[5] A. Di Matteo, I.A. Kougioumtzoglou, A. Pirrotta, P.D. Spanos, M. Di Paola, Stochastic response determination of nonlinear oscillators with fractional derivatives elements via the wiener path integral, Probab. Eng. Mech. 38 (2014) 127–135.
[6] A.F. Psaros, O. Brudastova, G. Malara, I.A. Kougioumtzoglou, Wiener path integral based response determination of nonlinear systems subject to non-white, non-Gaussian, and non-stationary stochastic excitation, J. Sound Vib. 433 (2018) 314–333.
[7] I.A. Kougioumtzoglou, A. Di Matteo, P.D. Spanos, A. Pirrotta, M. Di Paola, An efficient Wiener path integral technique formulation for stochastic response determination of nonlinear MDOF systems, J. Appl. Mech. 82 (10) (2015) 101005.
[8] A.F. Psaros, I.A. Kougioumtzoglou, I. Petromichelakis, Sparse representations and compressive sampling for enhancing the computational efficiency of the Wiener path integral technique, Mech. Syst. Signal Process. 111 (2018) 87–101.
[9] A.F. Psaros, I. Petromichelakis, I.A. Kougioumtzoglou, Wiener path integrals and multi-dimensional global bases for non-stationary stochastic response determination of structural systems, Mech. Syst. Signal Process. 128 (2019) 551–571.
[10] P. Hänggi, Path integral solutions for non-Markovian processes, Z. Phys. B 75 (2) (1989) 275–281.
[11] A.N. Drozdov, P. Talkner, Path integrals for Fokker–Planck dynamics with singular diffusion: Accurate factorization for the time evolution operator, J. Chem. Phys. 109 (6) (1998) 2080–2091.
[12] A. McKane, H. Luckock, A. Bray, Path integrals and non-Markov processes. I. General formalism, Phys. Rev. A 41 (2) (1990) 644.
[13] H.S. Wio, P. Colet, M. San Miguel, L. Pesquera, M. Rodriguez, Path-integral formulation for stochastic processes driven by colored noise, Phys. Rev. A 40 (12) (1989) 7312.
[14] P. Colet, H.S. Wio, M. San Miguel, Colored noise: A perspective from a path-integral formalism, Phys. Rev. A 39 (11) (1989) 6094.
[15] S. Einchcomb, A. McKane, Use of Hamiltonian mechanics in systems driven by colored noise, Phys. Rev. E 51 (4) (1995) 2974.
[16] F. Ikhouane, J. Rodellar, Systems with Hysteresis: Analysis, Identification and Control using the Bouc-Wen Model, John Wiley & Sons, 2007.
[17] I. Petromichelakis, A.F. Psaros, I.A. Kougioumtzoglou, Stochastic response determination and optimization of a class of nonlinear electromechanical energy harvesters: A Wiener path integral approach, Probab. Eng. Mech. 53 (2018) 116–125.
[18] P.D. Spanos, F.M. Strati, G. Malara, F. Arena, An approach for non-linear stochastic analysis of U-shaped OWC wave energy converters, Probab. Eng. Mech. 54 (2018) 44–52.
[19] F. Wiegel, Path integrals with topological constraints: Aharonov-Bohm effect and polymer entanglements, Physica A 109 (3) (1981) 609–617.
[20] S.N. Majumdar, Brownian functionals in physics and computer science, in: The Legacy of Albert Einstein: A Collection of Essays in Celebration of the Year of Physics, World Scientific, 2007, pp. 93–129.
[21] S.N. Majumdar, J. Randon-Furling, M.J. Kearney, M. Yor, On the time to reach maximum for a variety of constrained Brownian motions, J. Phys. A 41 (36) (2008) 365005.
[22] C.W. Gardiner, Handbook of Stochastic Methods for Physics, Chemistry and the Natural Sciences, third ed., in: Springer Series in Synergetics, vol. 13, Springer-Verlag, Berlin, 2004, p. xviii+415.
[23] L. Arnold, Stochastic Differential Equations: Theory and Applications, Dover Publications, New York, 1974.
[24] T.T. Soong, M. Grigoriu, Random Vibration of Mechanical and Structural Systems, Prentice Hall, New Jersey, 1992.
[25] I.I. Gihman, A.V. Skorohod, Stochastic Differential Equations, in: Ergebnisse der Mathematik und ihrer Grenzgebiete. 2. Folge, Springer-Verlag, Berlin Heidelberg, 1972.
[26] H. Risken, Fokker-planck equation, in: The Fokker-Planck Equation, Springer, 1996, pp. 63–95.
[27] L. Onsager, S. Machlup, Fluctuations and irreversible processes, Phys. Rev. 91 (6) (1953) 1505.
[28] M. Chaichian, A. Demichev, Path Integrals in Physics: Stochastic Processes and Quantum Mechanics, Institute of Physics Publishing, Bristol, U.K., 2001.
[29] H.S. Wio, Path Integrals for Stochastic Processes: An Introduction, World Scientific Pub Co Inc, 2013.
[30] M.F. Weber, E. Frey, Master equations and the theory of stochastic path integrals, Rep. Progr. Phys. 80 (4) (2017) 046601.
[31] L.F. Cugliandolo, V. Lecomte, F. Van Wijland, Building a path-integral calculus, 2018, arXiv preprint arXiv:1806.09486.
[32] F. Langouche, D. Roekaerts, E. Tirapegui, Functional integrals and the Fokker-Planck equation, Il Nuovo Cimento B (1971-1996) 53 (1) (1979) 135–159.
[33] A. Naess, V. Moe, Stationary and non-stationary random vibration of oscillators with bilinear hysteresis, Int. J. Non-Linear Mech. 31 (5) (1996) 553–562.
[34] J.B. Roberts, P.D. Spanos, Random Vibration and Statistical Linearization, in: Dover Civil and Mechanical Engineering, Dover Publications, Mineola, NY, 2003.
[35] R.P. Feynman, A.R. Hibbs, Quantum Mechanics and Path Integrals: Emended Edition, in: Dover Books on Physics, Dover Publications, 2010.
[36] H. Kleinert, Path Integrals in Quantum Mechanics, Statistics, Polymer Physics, and Financial Markets, World Scientific Pub Co Inc, 2009.
[37] G.M. Ewing, Calculus of Variations with Applications, Dover, New York, 1985.
[38] L.D. Elsgolc, Calculus of Variations, Dover Publications, Mineola, N.Y, 2007.
[39] I.A. Kougioumtzoglou, A Wiener path integral solution treatment and effective material properties of a class one-dimensional stochastic mechanics problems, J. Eng. Mech. 143 (6) (2017) 04017014.
[40] O.C. Zienkiewicz, Finite Elements and Approximation, Dover Publications, Mineola, N.Y, 2006.
[41] J. Nocedal, S. Wright, Numerical Optimization, in: Springer Series in Operations Research and Financial Engineering, Springer, New York, 2006.

[42] R. Storn, K. Price, Differential evolution–a simple and efficient heuristic for global optimization over continuous spaces, J. Global Optim. 11 (4) (1997) 341–359.
[43] C. Audet, J.E. Dennis Jr, Analysis of generalized pattern searches, SIAM J. Optim. 13 (3) (2002) 889–903.
[44] C. Lanczos, The Variational Principles of Mechanics, in: Dover Books on Physics, Dover Publications, Mineola, NY, 1986.
[45] M. Giaquinta, S. Hildebrandt, Calculus of Variations I, in: Grundlehren der mathematischen Wissenschaften, Vol. 1, Springer, Berlin, 2006.
[46] C.W. Gear, B. Leimkuhler, G.K. Gupta, Automatic integration of Euler-Lagrange equations with constraints, J. Comput. Appl. Math. 12 (1985) 77–90.
[47] G. Strang, Linear Algebra and its Applications, fourth ed., Thomson Higher Education, Belmont, CA, 2006.
[48] G.E. Shilov, Linear Algebra, in: Dover Books on Mathematics, Dover Publications, Mineola, NY, 1977.
[49] E.N. Antoniou, A.A. Pantelous, I.A. Kougioumtzoglou, A. Pirrotta, Response determination of linear dynamical systems with singular matrices: A polynomial matrix theory approach, Appl. Math. Model. 42 (2017) 423–440.
[50] R.H. Byrd, J. Nocedal, A tool for the analysis of quasi-Newton methods with application to unconstrained minimization, SIAM J. Numer. Anal. 26 (3) (1989) 727–739.
[51] D. Goldfarb, A family of variable-metric methods derived by variational means, Math. Comp. 24 (109) (1970) 23–26.
[52] D.C. Liu, J. Nocedal, On the limited memory BFGS method for large scale optimization, Math. Program. 45 (1–3) (1989) 503–528.
[53] M.R. Hestenes, Multiplier and gradient methods, J. Optim. Theory Appl. 4 (5) (1969) 303–320.
[54] R.T. Rockafellar, The multiplier method of hestenes and Powell applied to convex programming, J. Optim. Theory Appl. 12 (6) (1973) 555–562.
[55] M.J. Powell, A fast algorithm for nonlinearly constrained optimization calculations, in: Numerical Analysis, Springer, 1978, pp. 144–157.
[56] D.P. Bertsekas, Constrained Optimization and Lagrange Multiplier Methods, Athena Scientific, Nashua, NH, 1982.
[57] K. Kanai, Semi-empirical formula for the seismic characteristics of the ground, Bull. Earthq. Res. Inst. 35 (1957) 309–325.
[58] H. Tajimi, A statistical method of determing the maximum response of a building structure during an earthquake, in: Proc. 2nd World Conf. Earthq. Eng. 1960, pp. 781–797.
[59] R.W. Clough, J. Penzien, Dynamics of Structures, Computers & Structures, Inc., Berkeley, CA, 1995.
[60] G. Alotta, M. Di Paola, A. Pirrotta, Fractional Tajimi–Kanai model for simulating earthquake ground motion, Bull. Earthq. Eng. 12 (6) (2014) 2495–2506.
[61] M. Shinozuka, G. Deodatis, Simulation of stochastic processes by spectral representation, Appl. Mech. Rev. 44 (4) (1991) 191–204.
[62] R. Bouc, Forced vibrations of mechanical systems with hysteresis, in: Proc. of the Fourth Conference on Nonlinear Oscillations, Prague, 1967, 1967.
[63] Y.-K. Wen, Method for random vibration of hysteretic systems, J. Eng. Mech. Div. 102 (2) (1976) 249–263.
[64] J.E. Hurtado, A.H. Barbat, Equivalent linearization of the Bouc–Wen hysteretic model, Eng. Struct. 22 (9) (2000) 1121–1132.
[65] Y. Wen, Equivalent linearization for hysteretic systems under random excitation, J. Appl. Mech. 47 (1) (1980) 150–154.
[66] P. Spanos, I. Kougioumtzoglou, Harmonic wavelet-based statistical linearization of the Bouc-Wen hysteretic model, in: Proceedings of the 11th International Conference on Applications of Statistics and Probability in Civil Engineering, ICASP, vol. 11, 2011, pp. 2649–2656.
[67] K. Papakonstantinou, P. Dimizas, V. Koumousis, An inelastic beam element with hysteretic damping, Shock Vib. 15 (3, 4) (2008) 273–290.
[68] A. Charalampakis, V. Koumousis, A Bouc–Wen model compatible with plasticity postulates, J. Sound Vib. 322 (4–5) (2009) 954–968.
[69] Y. Wen, Methods of random vibration for inelastic structures, Appl. Mech. Rev. 42 (2) (1989) 39–52.
[70] M. Ismail, F. Ikhouane, J. Rodellar, The hysteresis Bouc-Wen model, a survey, Arch. Comput. Methods Eng. 16 (2) (2009) 161–188.